ENHANCING 3D SEISMIC DATA TO AID INTERPRETATION OF CREE SAND CHANNELS, OFFSHORE NOVA SCOTIA

APPROVED BY SUPERVISORY COMMITTEE:

_____

Sumit Verma, Ph.D.
Chair

_____

Joonghyeok Heo, Ph.D.

_____

Robert Trentham, Ph.D.

_____

Shawn Watson, Ph.D.
Graduate Faculty Representative

ENHANCING 3D SEISMIC DATA TO AID INTERPRETATION OF CREE SAND CHANNELS, OFFSHORE NOVA SCOTIA

By

RUSTAM KHOUDAIBERDIEV, B.Sc.

THESIS

Presented to the Graduate Faculty of Geology of

The University of Texas of the Permian Basin

In Partial Fulfillment

of Requirements

for the Degree of

MASTER OF SCIENCE

THE UNIVERSITY OF TEXAS OF THE PERMIAN BASIN

December 2018

DEDICATION

To Jacqui, a woman of good heart.

ACKNOWLEDGEMENTS

In appreciation of the unyielding support from my graduate committee, Dr. Sumit Verma, Dr. Joonghyeok Heo, Dr. Robert Trentham and Dr. Shawn Watson.

In further appreciation of my colleagues at school, Paritosh Bhatnagar, Craig Bennett and Sterling Lepard, whose assistance shaped my work.

ABSTRACT

Potential hydrocarbon reservoirs can be found within deltaic channels, these channels have the ability to form continuous transport systems for hydrocarbons. Distributary sand-filled channels, which generally have high porosity and high permeability sandstones, in particular can serve as excellent reservoirs. The sea level fall, or regression can change in sea level can move the delta system close to the This study is focused on the Penobscot field, located off of the eastern shores of Nova Scotia. The emphasis of this study is taking a detailed look into the sand channels within the Cree Sand of the Logan Canyon, creating a workflow for seismic data enhancement, as well as using similarity seismic attributes (coherence and coherent energy) to delineate these features.

Extensive studies have been performed in analysis of deltaic channel systems and their ability to act as reservoirs for hydrocarbons. The research will follow an equivalent approach, with an emphasis on petrophysical analysis, 3D seismic data conditioning (through an application of a seismic mute, prestack and poststack structure-oriented filtering) and attribute-assisted interpretation, to consequently identify and map sand channels.

TABLE OF CONTENTS

LIST OF TABLES

LIST OF FIGURES

CHAPTER I

INTRODUCTION

Deltaic channel systems are among the largest reservoirs for petroleum exploration in submarine environments. The Cree Sand of the Logan Canyon Formation at Penobscot in the Sable sub-Basin, offshore Nova Scotia, contains deltaic channels, giving it excellent reservoir potential. Although, there has been have studies in the past in Penobscot area, with the help of open source seismic and well logs released by Nova Scotia Department of Energy (Mandal and Srivastava, 2017; Qayyum et al., 2015, Qayyum et al., 2012), there has been no study on Logan Canyon formation. In this study, we make an effort to study Logan Canyon formation with seismic survey and well log data.

In general, distributary channels are formed through river bifurcation, or the splitting of a single river flow into multiple streams. As sediment flows into the delta, the coarsest sediments are quickly deposited in these channels due to the flow being too slow to carry sand-sized grains. Thus, deltaic distributary channels are typically filled with reservoir-grade sands (Slatt, 2006). The change in the relative seal level can changes the shore line, and also the position of the submarine delta.

Penobscot seismic survey is contaminated with coherent noise (Mandal and Srivastava, 2017). Marine seismic surveys are generally contaminated by a variety of noise, including different types of coherent and random noise. If the coherent noise is not properly suppressed, such noise appears as steeply dipping events on the processed NMO

corrected gathers (Cahoj et al, 2016). This can be seen as acquisition footprint on the stacked seismic data. Seismic attribute interpretation suffers greatly due to the presence of strong noise. Chopra and Marfurt (2007) showed that the steeply dipping noise can be reduced with structure-oriented filtering (SOF). Researchers, have applied different filters including mean, median, alpha-trimmed mean, LUM (lower-upper-middle), and principal component filtering (Zhang et al., 2016).

Seismic attribute interpretation through the use of similarity attributes can help delineate deltaic channels (Khoudaiberdiev et al., 2017). Coherence and coherent energy seismic attributes aid in interpretation of discontinuous features, which are not readily identifiable using alternative attributes. As a result, these seismic attributes have gained great prominence. Since their inception during the 1990s, they have become the favored tool for the mapping of stratigraphic depositional environments (Peyton et al., 1998). These advances in seismic attributes allow us to delineate in detail the subtle levees and fans of a deltaic system.

I employ seismic data conditioning such as a seismic mute and the aforementioned SOF (in Prestack and Poststack data) in order to enhance the 3D seismic dataset for subsequent channel delineation.

CHAPTER II

GEOLOGIC OVERVIEW

The Scotian Basin is located in offshore Nova Scotia, continuing approximately 746 miles from the Yarmouth Arch / United States border in the southwest, to the Avalon Uplift on the Grand Banks of Newfoundland in the northeast (Figure 1). The stratigraphic framework is episodic and dominated by a long history of passive-margin deposition. The Cree Sand of the Logan Canyon Formation is located at an approximated depth of 5,100 to 6,600 ft, with an overall thickness of 1,500 ft (Figure 2).

Building of the Scotian Basin began soon after the separation and rifting of the North American continent from the African continent, all during the break-up of Pangea. The Scotian Basin is made up of a series of depocenters and platforms, which includes the Sable Subbasin. Working in conjunction, the series of platforms and subbasins have significantly controlled sediment distribution for a period of over 190 million years. A detailed list of incipient rift basins can be seen in Figure 3.

Early deposition in the area is characterized by an initial transition (Anisian to Taorcian) from terrestrial rift sediments to shallow marine carbonates and clastics (NSDE, 2011). This is followed by an initial postrift carbonate-dominated sequence (Aalenian – Tithonian). The second postrift sequence (Berriasian – Turonian) consists of a thick, rapidly deposited deltaic wedge (Missisauga Formation) and a series of thinner, backstepping deltaic lobes (Logan Canyon Formation). These two deltaic formations are separated by the Naskapi Shale (Aptian MFS). There is an influx of coarser clastics (Cree

sands) that occasionally interrupt the deposition of transgressive shales. The Cree is the oldest deltaic member of the Logan Canyon formation, and thus contains the thickest and most abundant channel sand deposits. Sands are deposited along a wide coastal plain and the shallow shelf, which eventually is overtaken by deeper marine shales and limestones of the Dawson Canyon Formation. At the end of the Cretaceous, we see sea level rise and subsequent basin subsidence, as well as, deposition of chalky mudstones and marine marl that comprise the Wyandot formation (Figure 4).

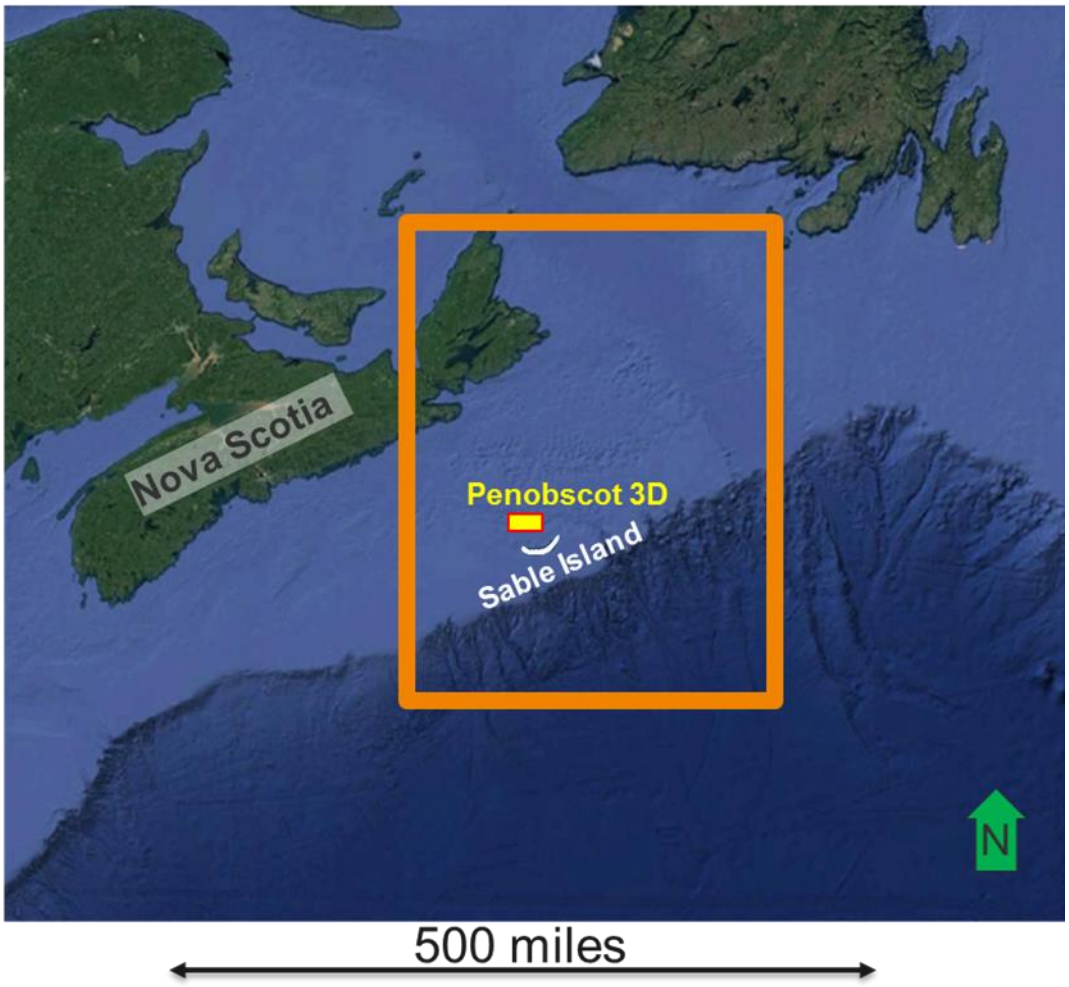

Figure 1. Location map of the study area (Google Earth Maps). The Penobscot 3D seismic survey is displayed in the yellow rectangle.

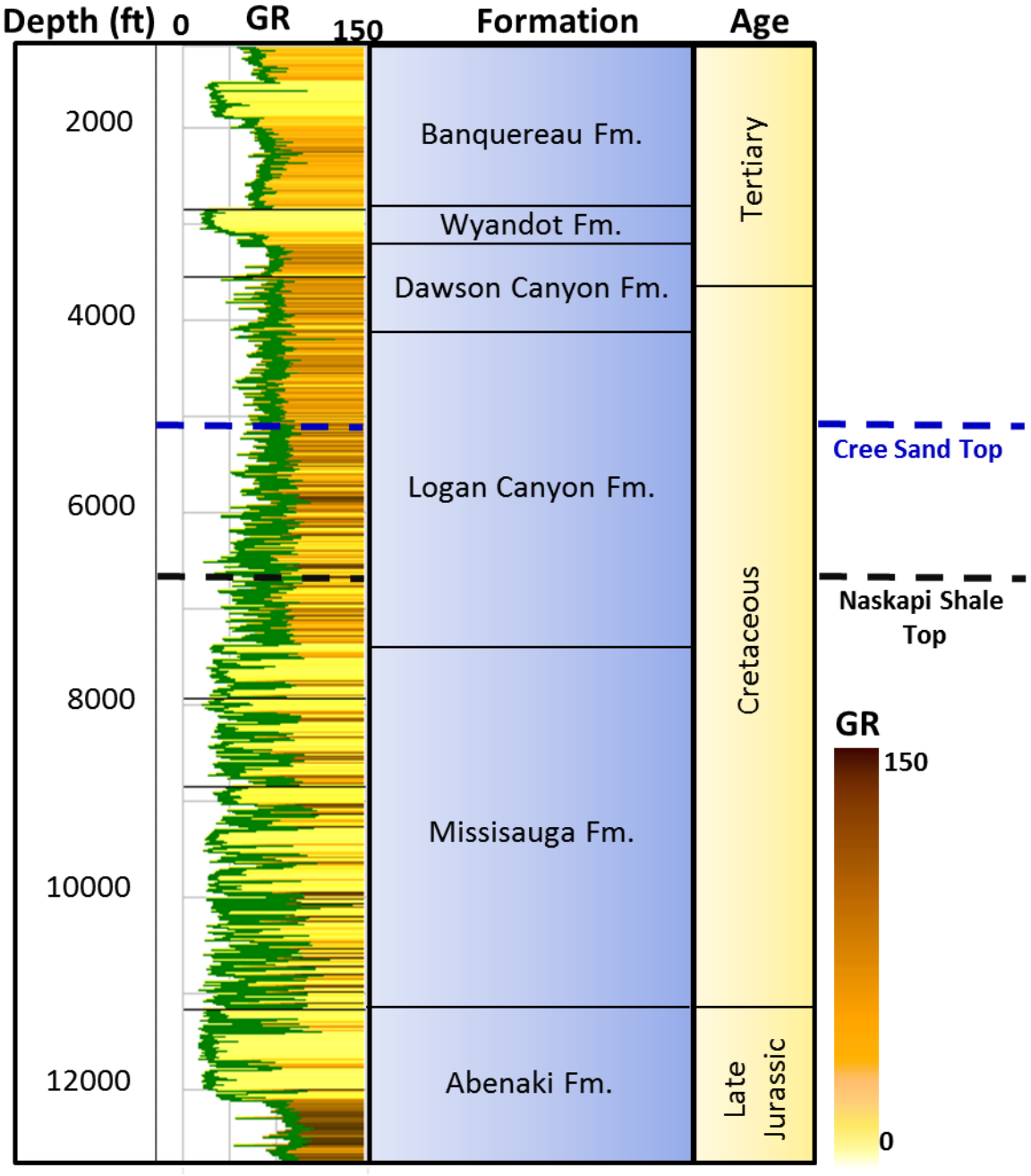

Figure 2. Stratigraphic column of the study area. The first track indicates measured depth. The second track shows the gamma ray log for well L-30, the darker color signifies high gamma ray values, which indicates shaly facies, whereas the light colors are for low gamma ray values, indicating sand rich facies. The third track shows the name of the formation and geological age (modified from Bhatnagar et al., 2017).

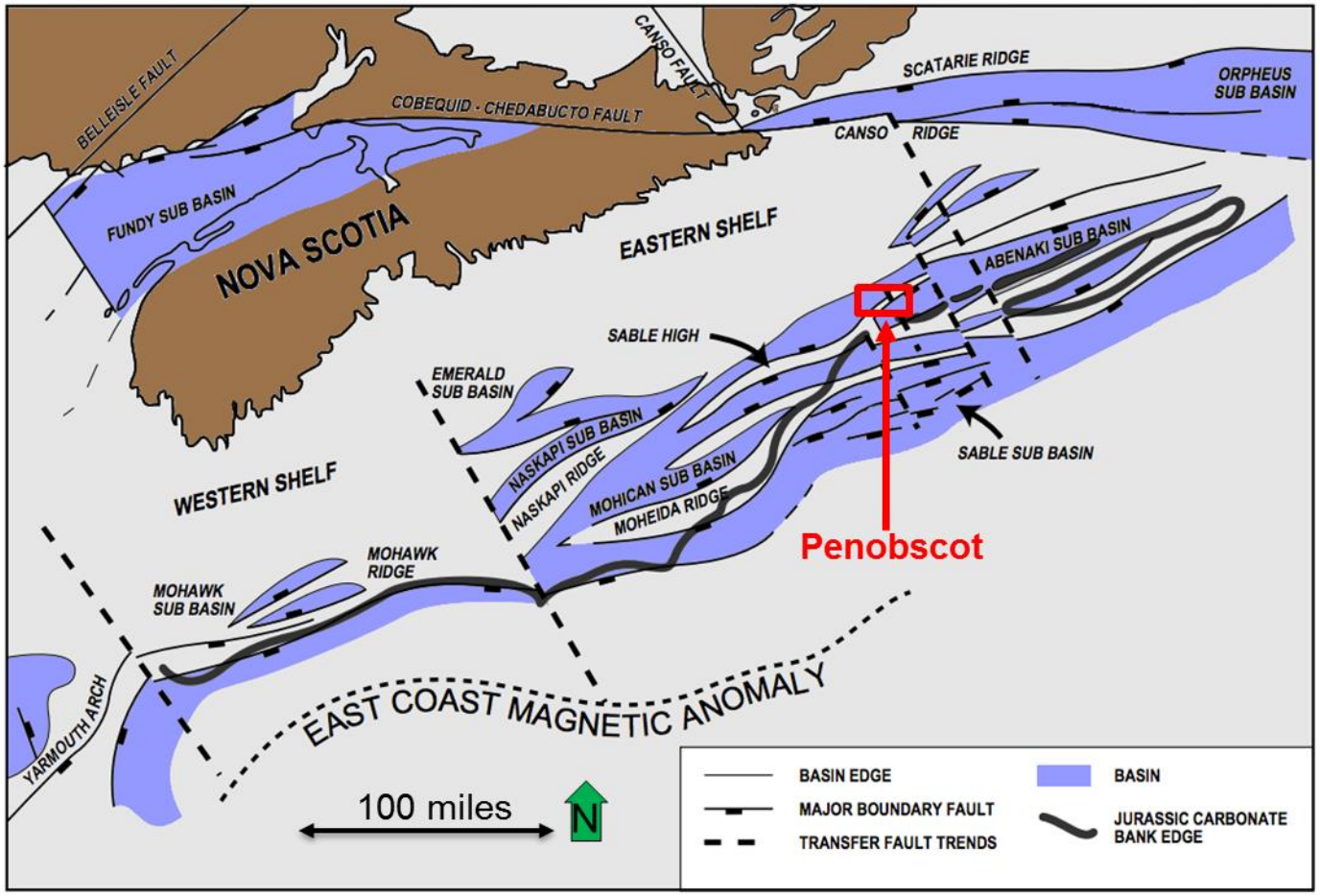

Figure 3. Building of the Scotian Basin with an outline of the survey area. The Scotian Basin is made up of a series of depocenters and platforms, which includes the Sable Subbasin. Working in conjunction, the series of platforms and subbasins have significantly controlled sediment distribution for a period of over 190 million years (modified from Piper, 1991).

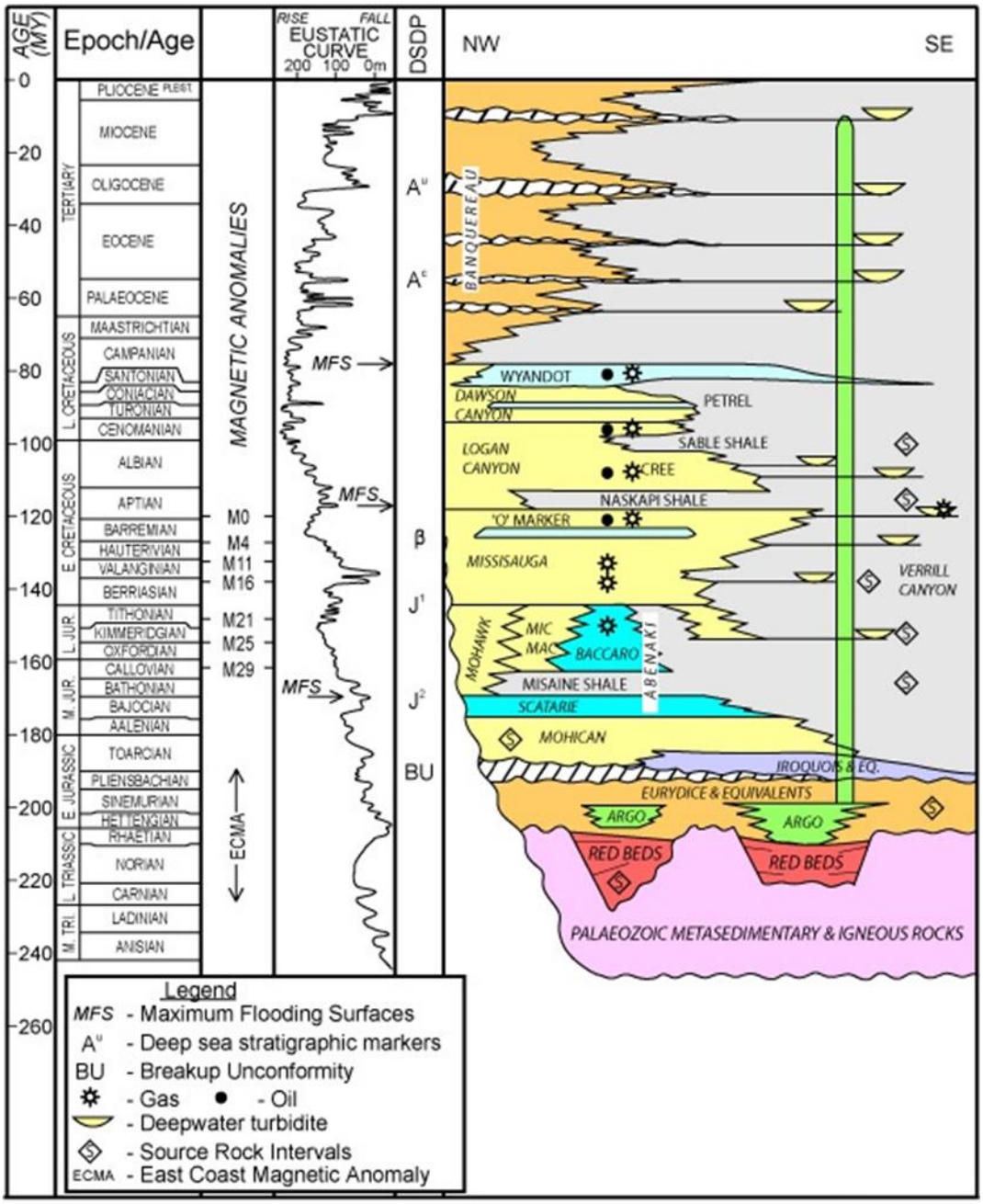

Figure 4. Stratigraphic column and sea level curve of the Scotian Basin (modified from CNSOPB, 2008).

CHAPTER III

PETROPHYSICAL ANALYSIS

Location of the wells and an outline of the 3D survey area can be seen in Figure 5. The dataset includes a full suite of logs and geologic tops (Table 1).

Well L-30 was spud in 1976 with a TD of 14,000 ft, containing an oil and gas show. Well B-41 was spud in 1977 with a TD of 11,300 ft, it was a dry hole (CNSOB, 2008). B-41 does not intersect a major sand channel of interest in this study and is the least relevant well, L-30 provides for a more detailed analysis of the sand channels. However, well L-30 has its limitation in its proximity to the major channels identified through the coherence and coherent energy attributes. The well intersects the very edge of a major channel, so facies change is not as readily identifiable.

The first step taken upon inspection of the logs was a quality check of the data. Relevant to the study intervals did not require adjustments.

As seen in Figures 6a, 6b and 6c, a detailed analysis of the wells provides an interpretation of facies changes and depositional environments in the Cree Sand (at an approximated 5,000 to 6,500 ft) and Naskapi Shale interval (approximately 6,925 to 7,390 ft). Naskapi Shale contains deepwater black shales at its base and pro-delta assemblages near the top (Figure 6a). In the Cree Sand section, depths where shale dominates give an indication of tide-dominated deltas, also observed is a fining upward sequence, indicating a larger quantity of channels at depth (Figures 6b and 6c).

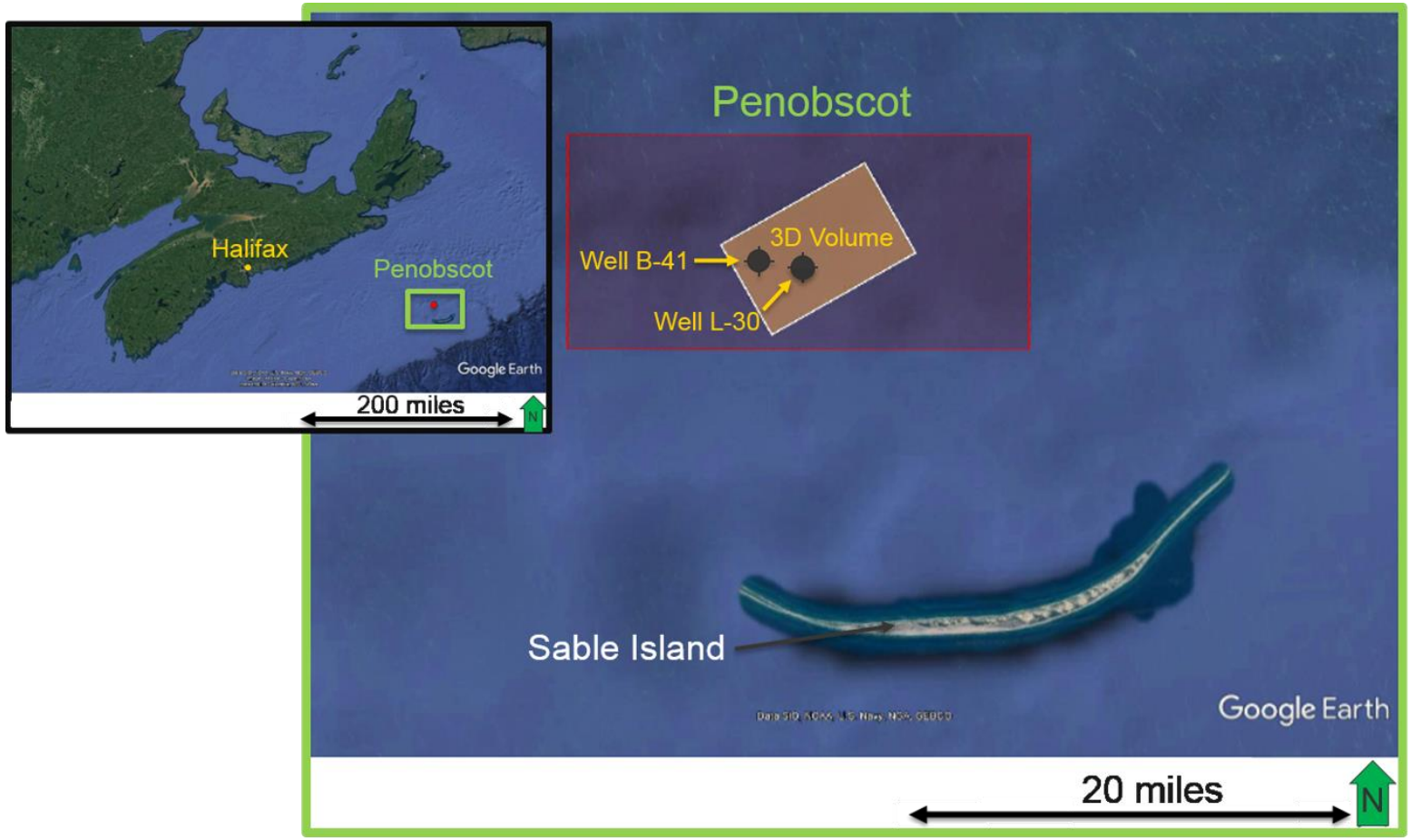

Figure 5. Location of the wells and the 3D survey area. Offshore Canada on the Scotian Shelf, located 15 miles off Sable Island and 170 miles from Halifax, Nova Scotia (Google Earth Maps).

Log	Well L-30	Well B-41
Caliper	X	X
Gamma Ray	X	X
Induction (Short, Medium, Deep)	X	X
Density	X	X
Neutron Porosity	X	X
Spontaneous Potential	X	X
Geological Tops	X	X

Table 1. Well logs. Wells L-30 and B-41 include a full suite of logs and their respective geological tops (CNSOPB, 2008).

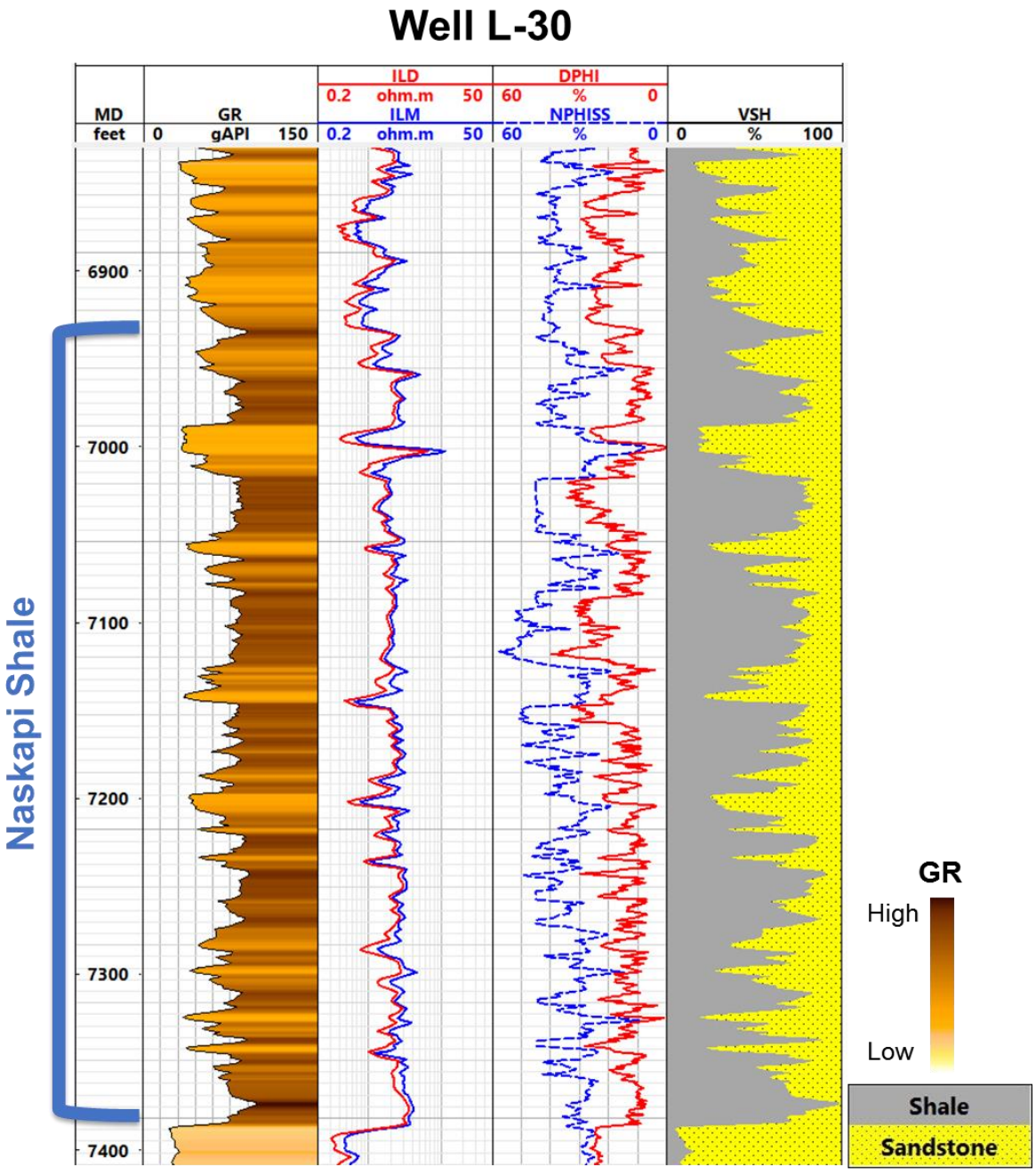

Figure 6a. Logs for well L-30. From left to right: Measured Depth, Gamma Ray, Resistivity (Deep and Medium), Density, Neutron Porosity (sandstone matrix) and Volume of Shale. Naskapi Shale interval (approximately 6,925 to 7,390 ft) contains deepwater black shales at its base and pro-delta assemblages near the top.

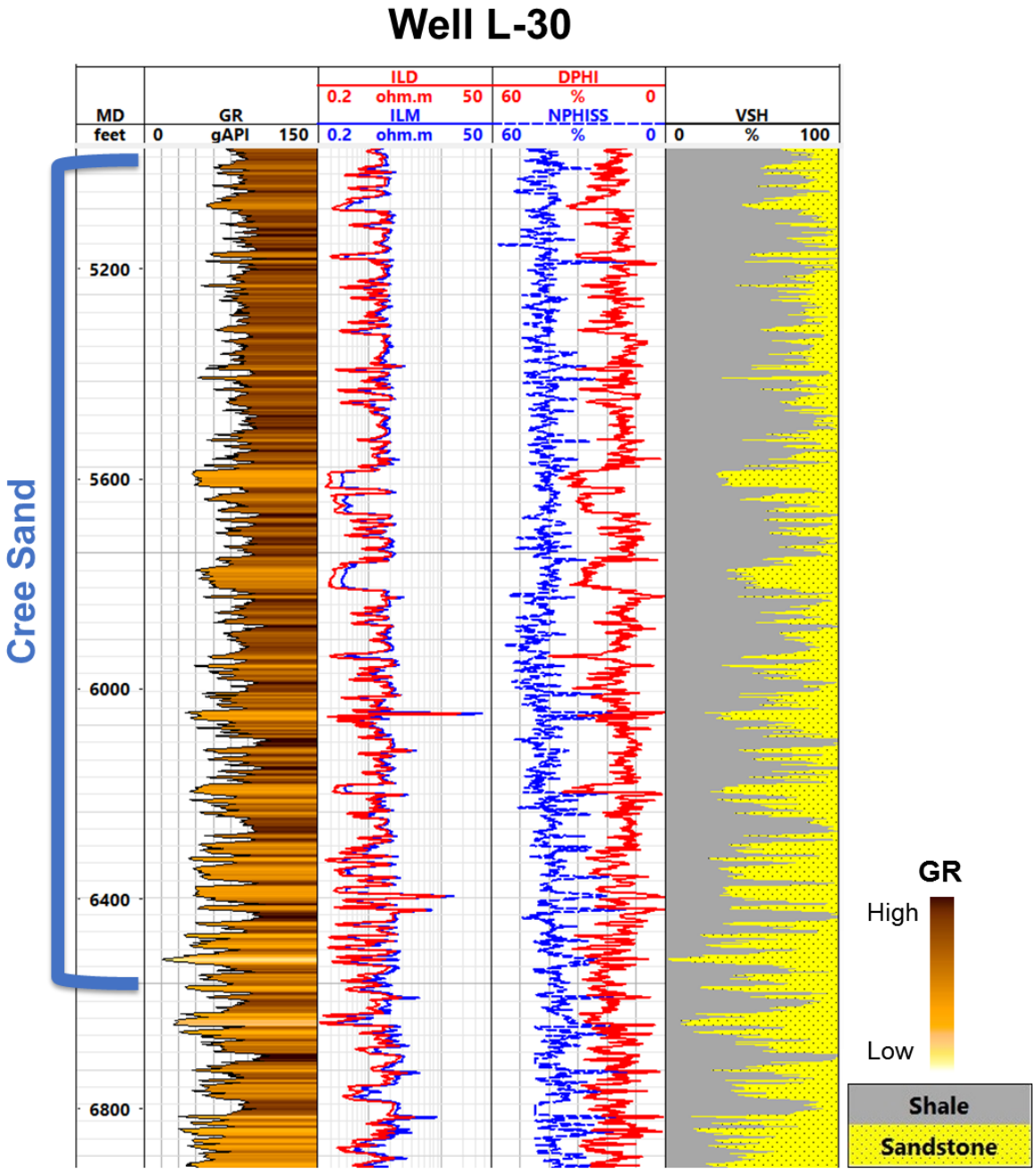

Figure 6b. Logs for well L-30. From left to right: Measured Depth, Gamma Ray, Resistivity (Deep and Medium), Density, Neutron Porosity (sandstone matrix) and Volume of Shale. In the Cree Sand section (at an approximated 5,000 to 6,500 ft), depths where shale dominates give an indication of tide-dominated deltas, also observed is a fining upward sequence, indicating a larger quantity of channels at depth.

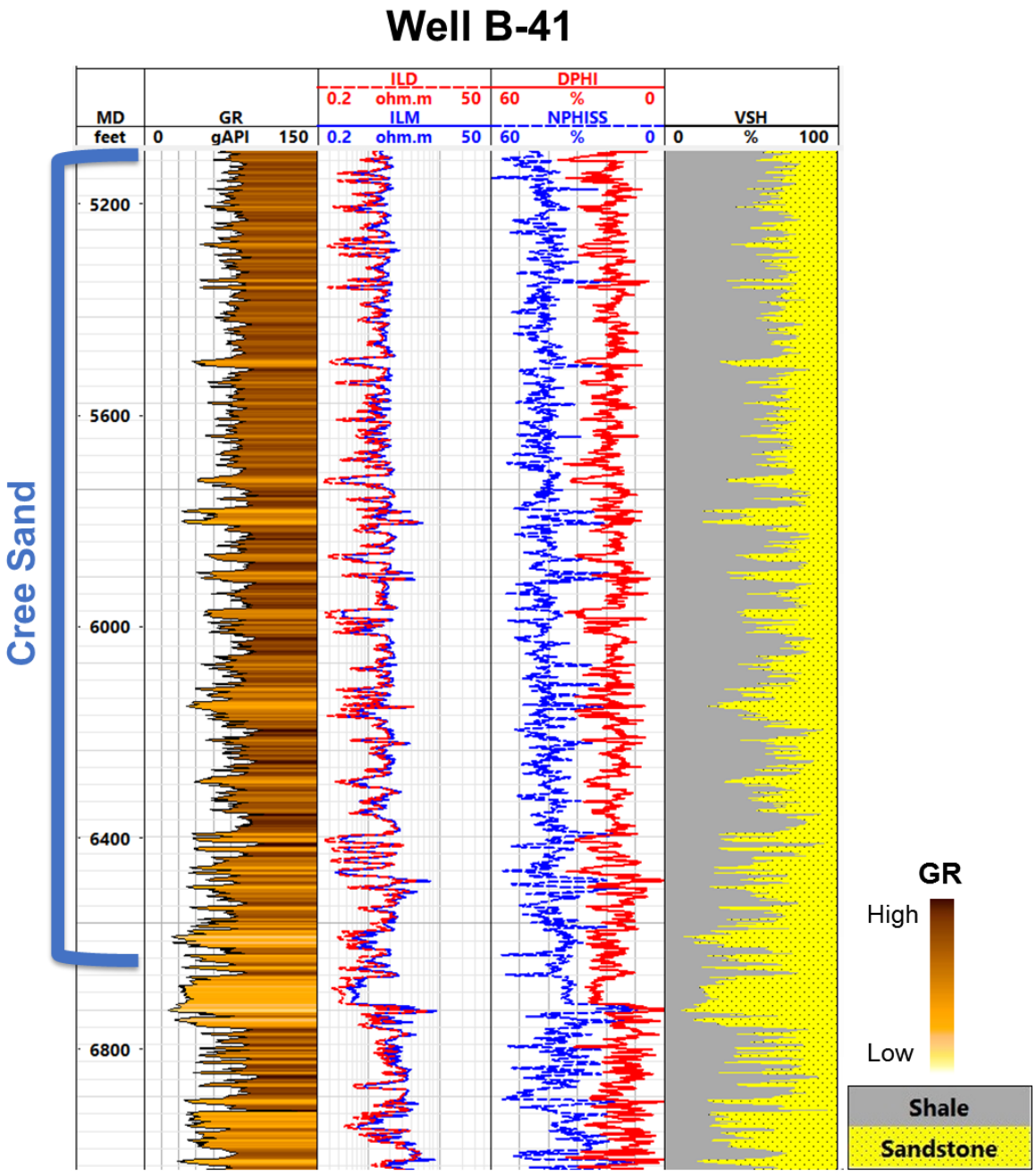

Figure 6c. Logs for well B-41. From left to right: Measured Depth, Gamma Ray, Resistivity (Deep and Medium), Density, Neutron Porosity (sandstone matrix) and Volume of Shale. In the Cree Sand section (at an approximated 5,000 to 6,500 ft), depths where shale dominates give an indication of tide-dominated deltas, also observed is a fining upward sequence, indicating a larger quantity of channels at depth.

CHAPTER IV

3D SEISMIC DATA QUALITY

The 3D seismic survey is located on the Scotian Shelf, offshore Canada. Seismic data is of moderate quality. The survey area is approximately 33.4 mi^2. It was acquired in 1992 with Pre Stack Time Migration (PSTM) and a 4 ms sample rate (Table 2). The version made available and subsequently processed is in December of 2007. This version is be used in this study.

Processing of acquired data was performed for the Offshore Energy Technical Research Association by Kelman Seismic Processing in December 2007. It includes surface related multiple elimination (wave equation KTI), Random Noise Suppression, Linear Noise Subtraction, Multiple Attenuation (Hyperbolic Radon), Pre Stack Time Migration (Kirchhoff method), NMO, and other methods (Table 3).

Inline Range	1000 - 1600 (step 1)
Crossline Range	1000 - 1481 (step 1)
Bin size (m) [inl/xl]	12.01 x 25.01
Z Range (ms)	0 - 6000 (step 4)
Seismic Polarity	SEG Normal
Size (km)	7.2 x 12.03
Sample Rate (ms)	4
Format	Pre Stack Time Migration (PSTM)
Version	True Amplitude and NMO Applied

Table 2. 3D Survey Parameters (CNSOPB, 2008).

1. Reformat to KTI Internal Format
2. Navigation Merge & Geometry
3. Designature Processing
4. Surface Related Multiple Elimination (wave equation KTI)
5. Random Noise Suppression
6. Adjacent Trace Stacking
7. Predictive Deconvolution: Length = 164ms, Gap = 32ms
8. Surface-Consistent Scaling
9. Velocity Analysis 0.5km
10. Linear Noise Subtraction
11. Multiple Attenuation (Hyperbolic Radon)
12. Velocity Analysis 0.5km
13. Bin Interpolation: Delaunay Triangulation Method
14. Pre Stack Time Migration: Method Kirchhoff Max Angle 65 Degrees, Apertura 4100m Output Offset Panels 175m - 3175m With Bin Size 50m
15. Velocity analysis 0.5km
16. NMO
17. SEGY output sorted by major X minor Y

Table 3. Processing History. Processed for the Offshore Energy Technical Research Association. Processed by Kelman Seismic Processing, December 2007. Project Penobscot-3D. Described is all of the processing done since the data was acquired (CNSOPB, 2008).

CHAPTER V

METHODOLOGY

A workflow is presented to illustrate the steps taken during data conditioning. A systematic approach was performed to generate results to meet with the studies objective. It is important to note that multiple iterations of the final Structure-oriented Filtering (SOF) are necessary to create an adequate balance of signal-to-noise for the final interpretation (Figure 7).

All steps are performed in the Attribute Assisted Seismic Processing & Interpretation (AASPI) software, a proprietary software belonging to the ConocoPhillips School of Geology & Geophysics at The University of Oklahoma. The version of AASPI used throughout is October 11th 2017.

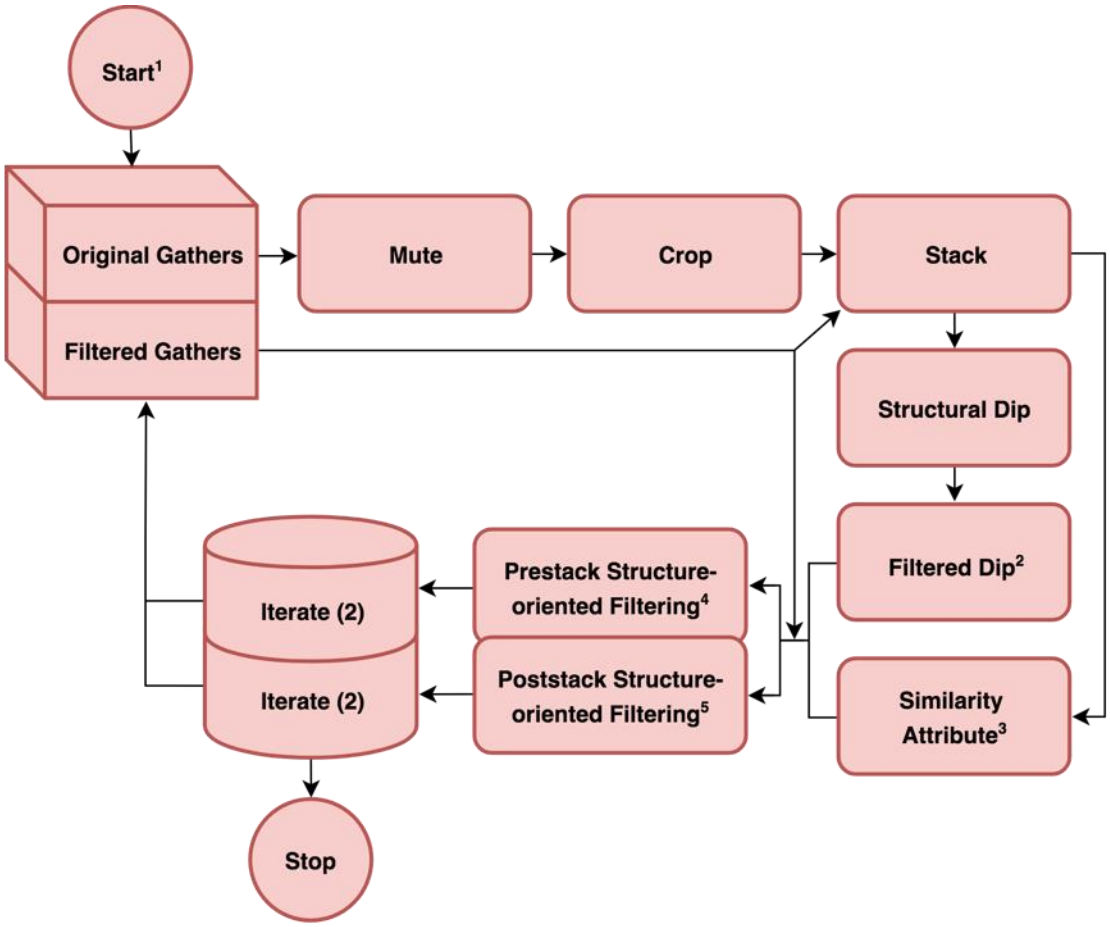

Figure 7. Workflow steps during data conditioning. Expanded descriptions of the steps is listed as their respective superscripts. (1) Start: Import prestack data to AASPI, convert SEGY to AASPI format. (2) Filtered Dip: Possible filters include LUM (lower-upper-middle), MSMTM (multistage median-based modified trimmed mean),median and mean filters. (3) Similarity Attribute: Possible products include Energy Ratio, Outer Product, Sobel Filter, Gradient Component, Total Energy and Coherent Energy. (4) Prestack Structure-oriented Filtering: Possible filtered attribute volumes include Principal Component, Alpha-Trimmed-Mean, Lower-Upper-Median and Mean. (5) Poststack Structure-oriented Filtering: This step will not require running Stack during iteration. Product options will be the same as Prestack SOF shown above.

WELL-TO-SEISMIC TIES

To calibrate seismic horizons with well tops and seismic derived attributes with well log properties, a well to seismic tie is performed. This in turn ensures an accurate time-depth relationship. The two available wells (L-30 and B-41) each generated synthetic data to best match the seismic data located at the well location. Well L-30 generated a 70% correlation and well B-41 had a 56% correlation. Our synthetic ties provided a good quality match with the seismic data (Figure 8).

Figures 9a and 9b provide a clearer image of the success in the well-to-seismic tie, namely for well L-30. Figure 9a displays a time structure slice of the Petrel formation (located at approximately 1,100 ms), which is a Late Cretaceous chalk and is the most prominent seismic marker above the Cree Sand. Figure 9b contains the seismic amplitude section AA' with a transposed gamma ray log from well L-30 and provides an indication of the success of the well-to-seismic tie.

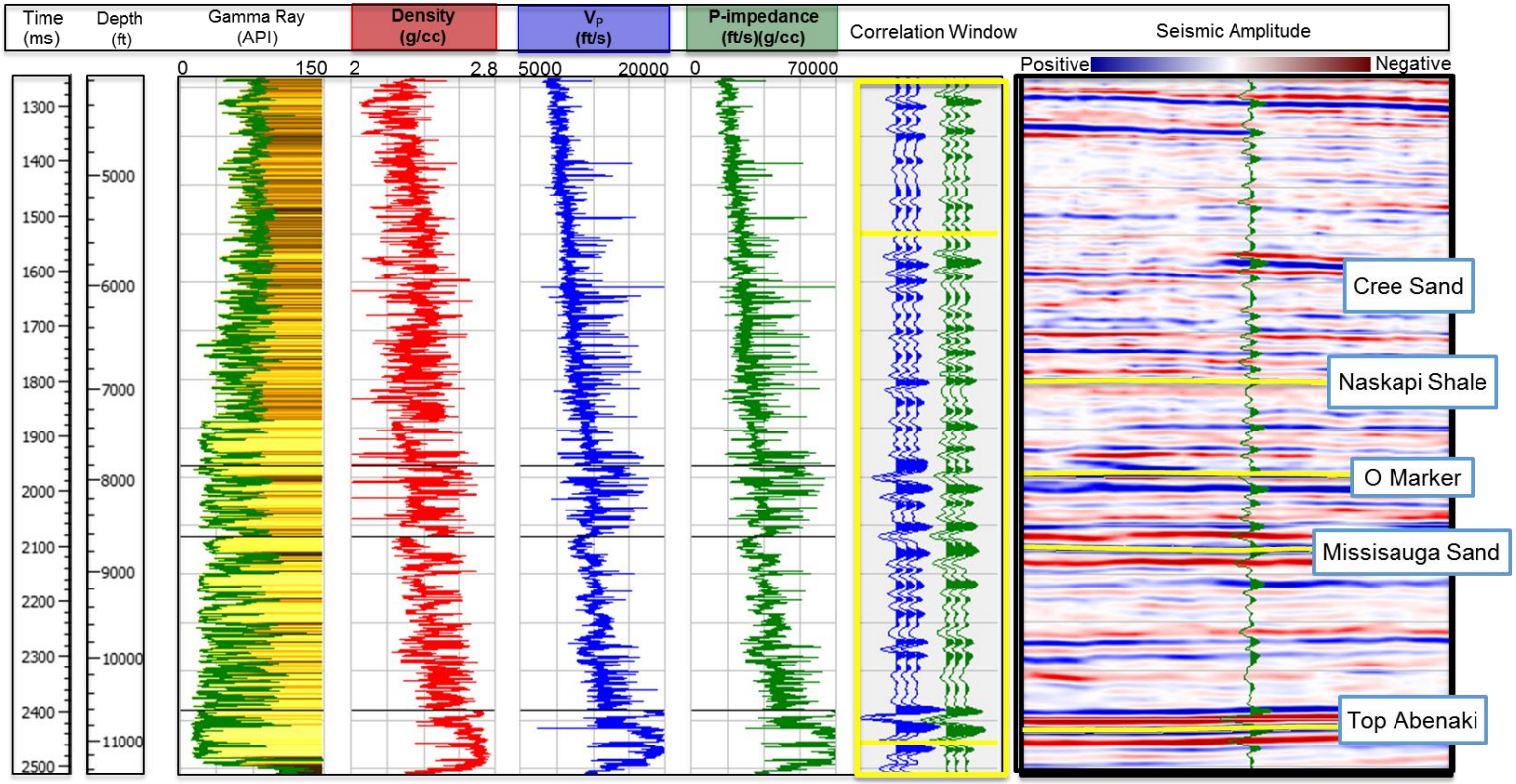

Figure 8. Well-to-seismic tie of well L-30. From left to right: Time, Depth (ft), Gamma Ray, Density, Seismic Velocity (Vp), Acoustic P-wave Impedance, Correlation Window (seismic generated in blue, well generated in green), Seismic Amplitude, Tops (from dataset). Synthetic tie provides a good quality match with the seismic data, for a correlation of 70%.

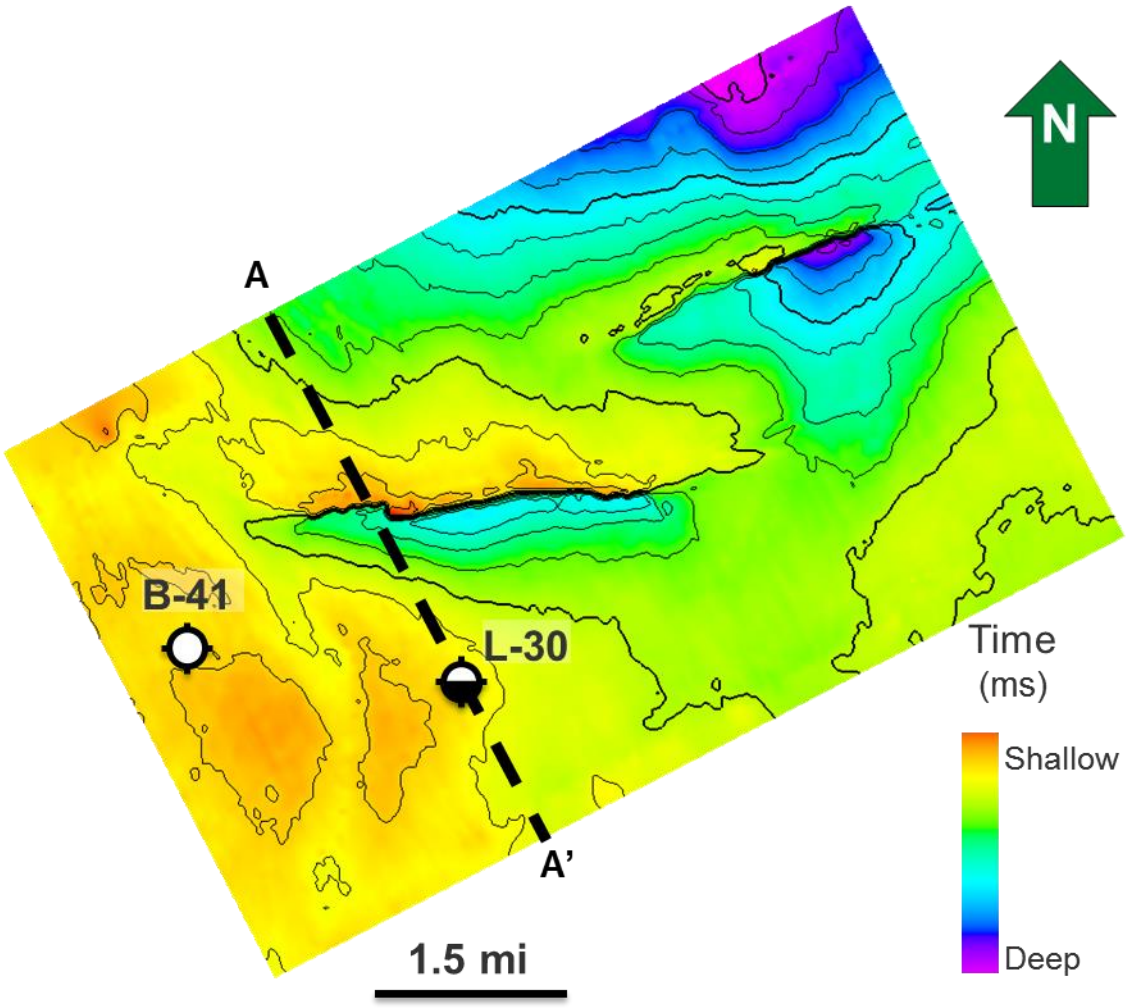

Figure 9a. Time structure slice of the Petrel formation. Located at approximately 1,100 ms, the Petrel formation is a Late Cretaceous chalk and is the most prominent seismic marker above the Cree Sand. Wells L-30 and B-41 are shown as a well symbols and A to A' is the location of cross-section 8b (modified from Khoudaiberdiev et al, 2017).

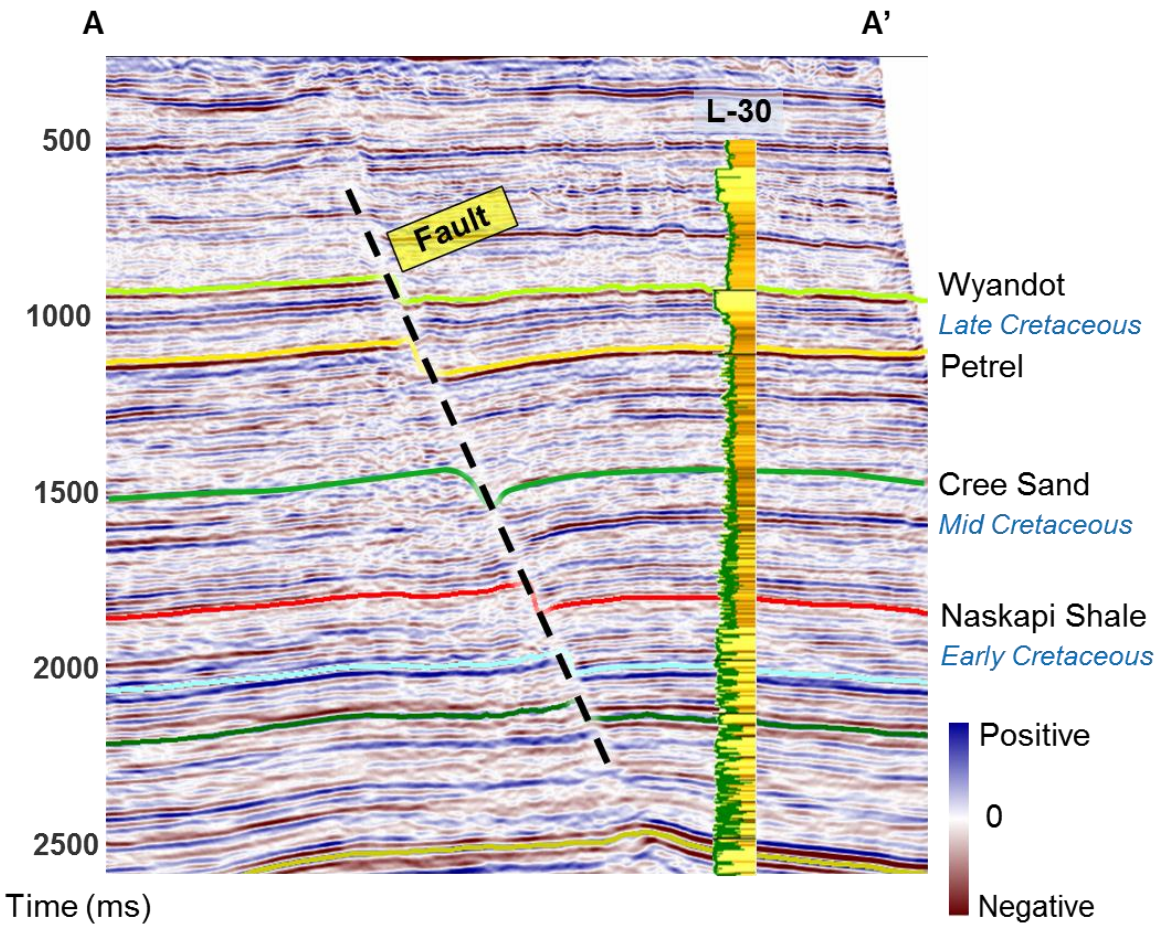

Figure 9b. Seismic amplitude section AA'. Gamma ray log from well L-30 is transposed onto a seismic cross-section and provides an indication of the well-to-seismic tie. Annotations on the right hand side indicate the name of the formation tops (in black regular font) and their ages (in light blue italics font) (modified from Khoudaiberdiev et al, 2017).

SIMILARITY

In order to aid the interpretation of sand channels, a similarity attribute will be used for direct analysis and as a tool for comparison of the impact of parameters to make a choice between output products. Based on an analysis of the 6 similarity products (Energy Ratio, Outer Product, Sobel Filter, Gradient Component, Total Energy and Coherent Energy) available in the Attribute Assisted Seismic Processing & Interpretation (AASPI) software, the 2 chosen for this are Outer Product and Coherent Energy. Outer Product (will be referred to as Coherence from now on) outcompetes the other products due to the results showing a desirable output of a greater spread of the data throughout the dataset. Coherent Energy is unique in its class since it is able to be plotted against a coherence volume to further enhance delineation of discontinuous features.

The coherence attribute is derived through a measure of the change in seismic amplitude and waveform shape, while a coherent energy attribute is created by a computation of the energy of the coherent component of a given seismic reflector in a set analysis window (DelMoro et al., 2013). Since channels will often display a sharp lateral shift in amplitude and waveform shape, they will be readily identifiable with a coherence attribute as continuous features that contrast nearby features. Coherent energy allows the delineation of high amplitude continuous features such as sands with high porosity overlying impermeable shales, to be displayed with a high coherent energy, and vice versa, a low amplitude continuous or discontinuous feature such as identically stacked shales, to be displayed with low coherent energy.

SEISMIC MUTE

Seismic data contains signals that are not desirable for an interpreter, in order to aid interpretation, a seismic mute is applied to a prestack dataset. By setting all trace values for offsets (source to receiver distance) beyond a certain offset and two-way time curve to zero, a mute is able to remove traces that are heavily contaminated with signals from multiples, water column noise, refractions and others (Bacon, Redshaw, & Simm, 2007). The application of a mute further assists in the computational time necessary to complete the Structure-oriented Filtering workflow, this is due to the decreased overall amount of traces.

Table 4 describes the offset vs. time mute pick parameters. Picks were made to remove far offset traces while preserving channel data in the Cree Sand interval (located at approximately 1500 to 1760 ms).

Figure 10 displays a pair (original on the top and muted on the bottom) of 3 seismic amplitude panels. Mute consideration included the location of the Cree Sand interval (approximately 1.5 to 1.8 s) and achieving an optimum signal-to-noise ratio for channel data preservation.

To display the results of the mute application, a coherence volume is used. Figure 11 shows the original and muted coherence volumes at 1,536 ms. What is observed is a direct impact of the applied mute on the seismic data set, namely the effect on channel delineation. Of note is the loss of some amplitude data in the top left, top right and bottom middle shown in the coherence volume with mute applied (these areas contained

only far offset amplitude data and were adversely muted). When applied to the original data set (top row), the results of the application of mute (bottom row) is a consistently cleaner channel display. Green box displays a zoomed in section of a major channel and blue arrows indicate channel edge improvements. Channels interpretation is shown as a red dashed line.

Offset Bin	Time (ms)
32	0
32	1400
37	1860
37	3000

Table 4. Offset (source to receiver distance) vs. Time (two–way travel time in seconds) mute pick parameters. Picks were made to remove far offset traces while preserving channel data in the Cree Sand interval (located at approximately 1500 to 1760 ms).

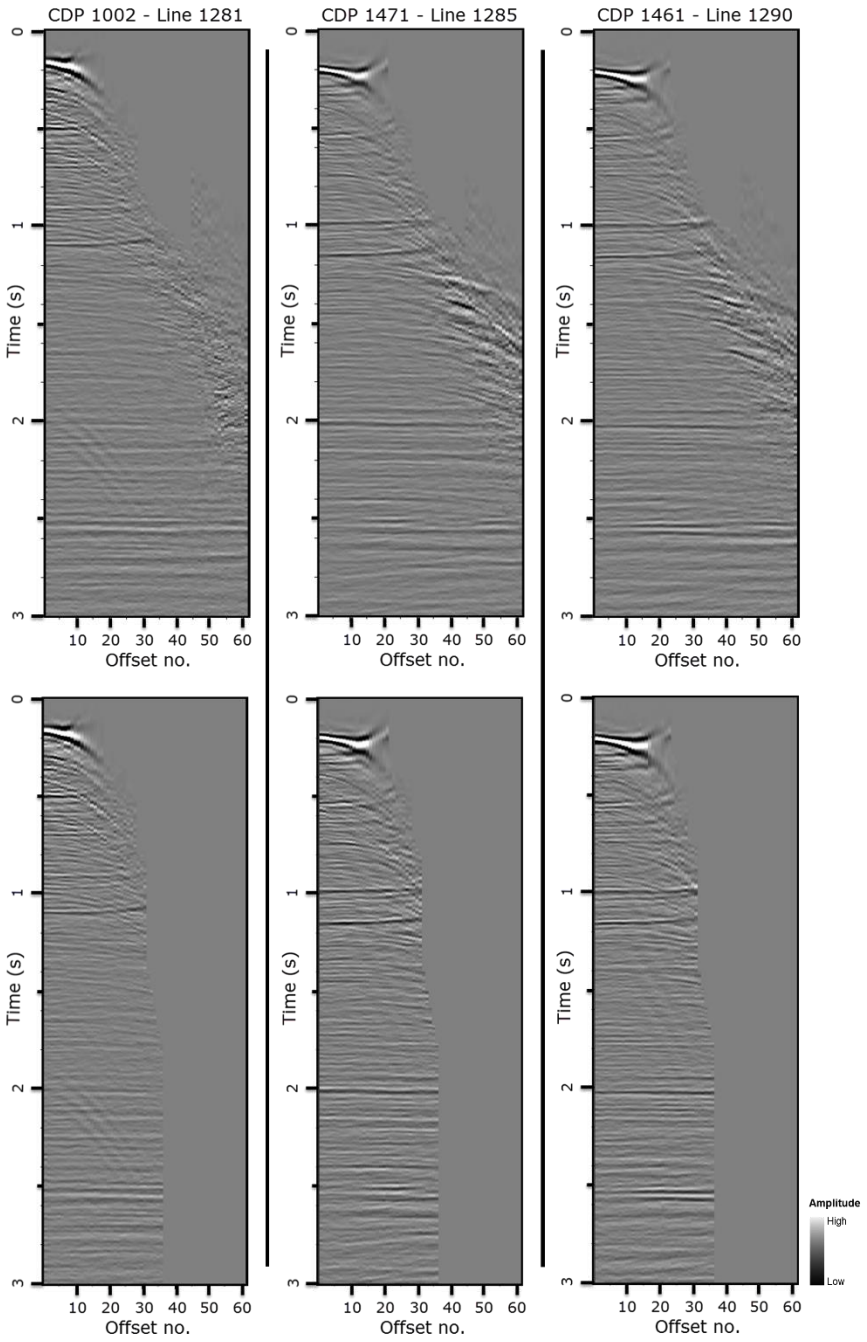

Figure 10. Original and muted seismic amplitude panels. Displayed are pairs (unmuted on the top and muted on the bottom) of 3 seismic amplitude gathers. Mute consideration included the location of the Cree Sand interval (approximately 1.5 to 1.8 s) and achieving an optimum signal-to-noise ratio for channel data preservation.

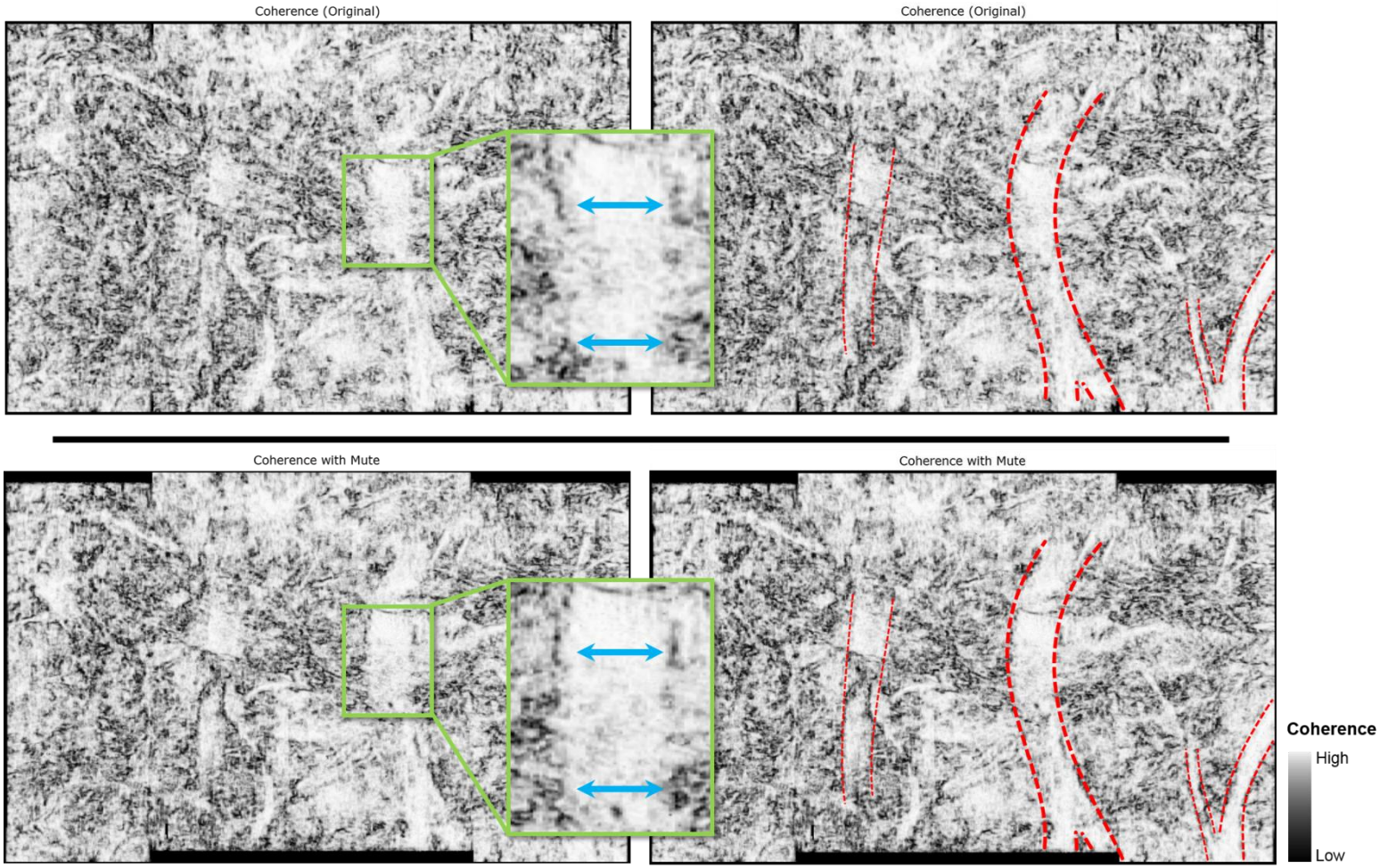

Figure 11. Original and muted coherence volumes (1,536 ms). Displayed is a direct impact of the applied mute on the seismic data set, namely the effect on channel delineation. Of note is the loss of some amplitude data in the top left, top right and bottom middle shown in the coherence volume with mute applied (these areas contained only far offset amplitude data and were adversely muted). When applied to the original data set (top row), the results of the application of mute (bottom row) is a consistently cleaner channel display. Green box displays a zoomed in section of a major channel and blue arrows indicate channel edge improvements. Channels interpretation is shown as a red dashed line.

PRESTACK STRUCTURE ORIENTED FILTERING

Structure-oriented Filtering (SOF) is performed through an accurate estimation of reflector dip, which is then followed by an application of a filter. The objective of SOF is the removal of random noise, suppression of coherent acquisition information, as well as, processing and migration artifacts that can interfere with reflectors that are important to an interpreter. Prestack SOF is designed to preserve edge data by applying an algorithm to prestack gathers whose coherency is greater than a user-defined parameter. The 5 filters available include mean, median, alpha-trimmed mean, LUM (lower-upper-middle), and principal component filtering (Zhang et al., 2016).

Shown in Table 5 are all of the Prestack SOF parameters and values used in the workflow steps (shown in Figure 7) during data conditioning. If a parameter is not listed in the table, the default values was used.

Prestack SOF (first and second iteration) coherence volumes are generated using a 20 percentile Alpha-Trimmed Mean filter. Results of the first iteration show a slight improvement in the signal-to-noise ratio (the “slightness” can be attributed to the non-aggressive similarity filter controls described in Table 5) and cleaner channel edges, this comes at a minor expense of internal channel detail and finer edge loss. Overall increase in continuity of previously interpreted channels allows for continued iteration. Results of the second iteration continue to build on the improvements of the first iteration seen in Figure 12, mostly notably channel continuity (seen in blue oval), albeit with very minor enhancement. This step will serve as a stopping point for Prestack Structure-oriented

Filtering due to continued iterations resulting in signal removal (particularly internal channel detail) with no significant improvement in channel edge detection (Figures 12 and 13).

Step	Parameter	Value
Stack	All	Default
Structural Dip	Theta max (degrees)	20
	Delta theta (degrees)	4
	Conversion velocity (m/s)	4000
	Dip window height (s)	0.02
	Inline window radius (m)	25.0005
	Crossline window radius (m)	12.5129
	Use rectangular window	Yes
	Analytical semblance (s_upper)	0.95
	Use L1-norm	Yes
Filtered Dip	Filter	Alpha-Trimmed Mean
	Lower and upper percentile	20
	Window length (m)	25
	Window width (m)	12.5
	Window height (s)	0.02
	Use rectangular window	Yes
Similarity	Desired attributes	Outer Product and Coherent Energy
	Use rectangular window	Yes
Prestack SOF	Rectangular window	Yes
	Inline window radius (m)	25.0005
	Crossline window radius (m)	12.5129
	Offset window radius (no. of traces)	2
	Filter control by similarity s_low	0.8
	Filter control by similarity s_high	0.9
	Filter control by similarity s_centered	0.95
	Filter	Alpha-Trimmed Mean

Table 5. Prestack Structure-oriented Filtering (SOF) parameters and values used in the workflow steps (shown in Figure 7) during data conditioning. All parameters not specified are default values.

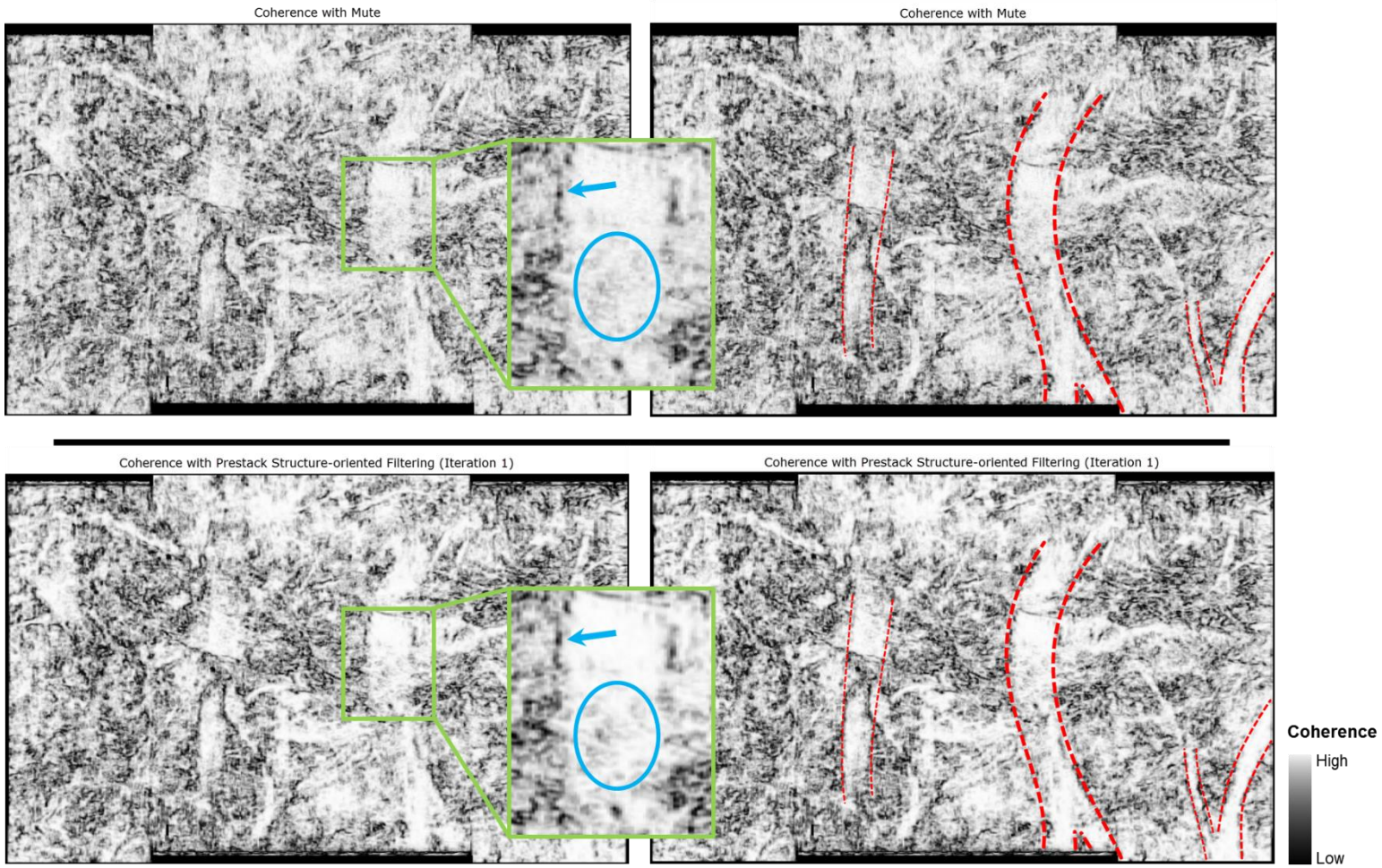

Figure 12. Muted and Prestack Structure-oriented Filtering (first iteration) coherence volumes (1,536 ms). Prestack SOF filter used is a 20 percentile Alpha-Trimmed Mean. Results of the first iteration show a slight improvement in channel coherence seen in the blue oval (the "slightness" can be attributed to the non-aggressive similarity filter controls) and cleaner channel edges seen with the blue arrow, this comes at a minor expense of internal channel detail and finer edge loss. Overall increase in continuity of previously interpreted channels allows for continued iteration.

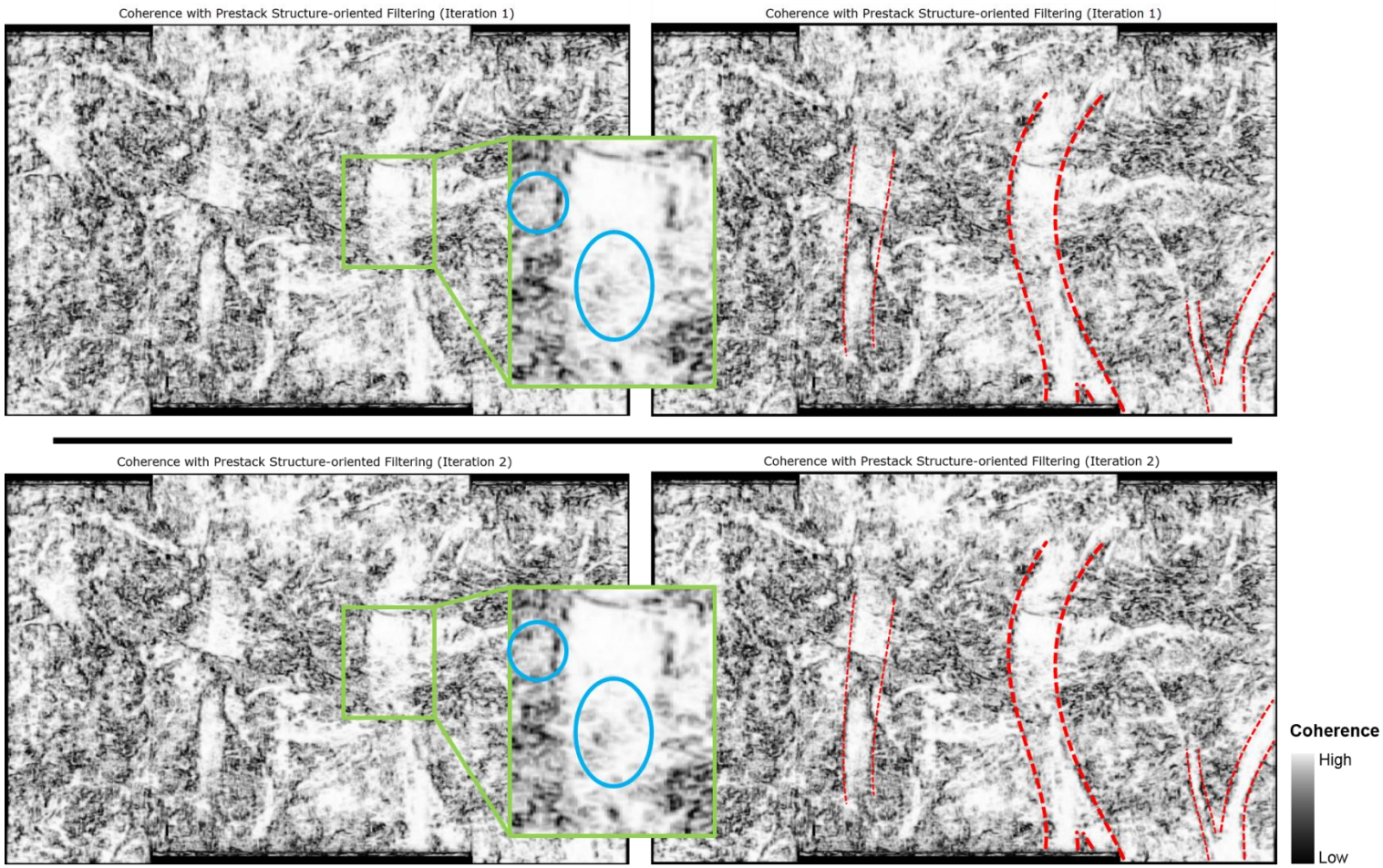

Figure 13. Prestack Structure-oriented Filtering (first iteration on top and second iteration on the bottom) coherence volumes (1,536 ms). Prestack SOF filter used is a 20 percentile Alpha-Trimmed Mean. Results of the second iteration continue to build on the improvements of the first iteration seen in Figure 12, mostly notably channel continuity (seen in blue oval), albeit with very minor enhancement. This step will serve as a stopping point for Prestack Structure-oriented Filtering due to continued iterations resulting in signal removal (particularly internal channel detail) with no significant improvement in channel edge detection.

POSTSTACK STRUCTURE ORIENTED FILTERING

Identical in its purpose to Prestack Structure-oriented Filtering (SOF), Poststack SOF is designed to preserve edge data through an application of an algorithm, in this case, to stacked gathers whose coherency is greater than a user-defined parameter (Zhang et al. 2016). The 5 filters available in Prestack SOF are the same as those in Poststack SOF.

Also nearly identical is the parameterization of Poststack SOF, with the only exception being the exclusion of the Stack step (Table 5) and the "Offset window radius" option not being available altogether due to the data being stacked. The 2 parameters will define the difference between prestack and poststack filtering. Stacking inherently acts as a filter, reducing the presence of noise at the risk of losing prominence in relevant areas of interest, this in turn shift the analysis capability of Poststack SOF.

Poststack SOF (first and second iteration) coherence volumes are generated using a 20 percentile Alpha-Trimmed Mean filter. Results of the first iteration show a slight improvement in channel edges seen with the blue arrows, but most notably, greatly increased internal channel detail seen with the blue oval. Overall increase in continuity of previously interpreted channels allows for continued iteration. Results of the second iteration continue to build on the improvements of the first iteration seen in Figure 14, mostly notably edge detection and internal channel detail. This step will serve as a stopping point for Poststack Structure-oriented Filtering due to continued iterations resulting in miniscule improvements in channel edge detection (Figures 14 and 15).

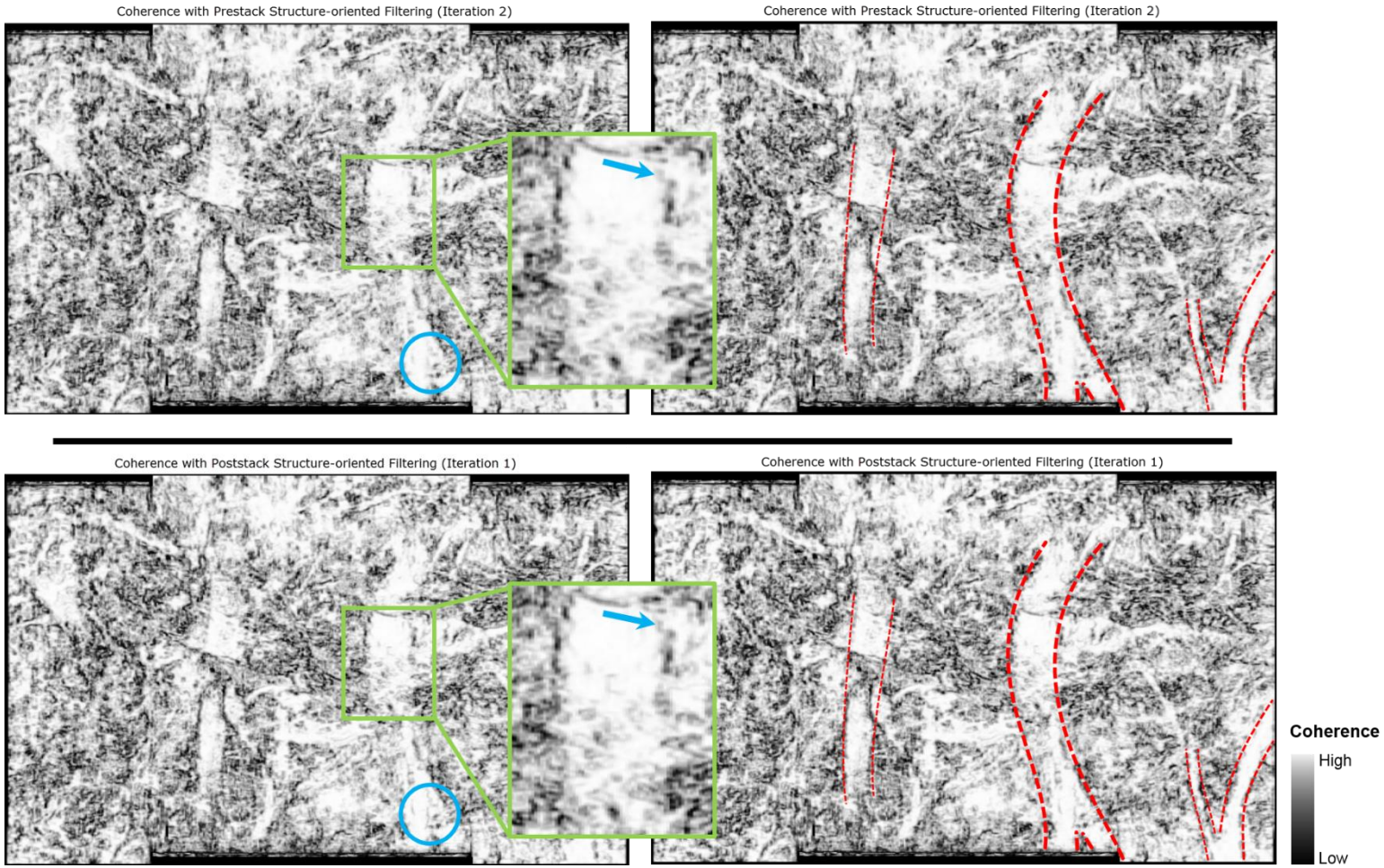

Figure 14. Prestack Structure-oriented Filtering (second iteration on top) and Poststack Structure-oriented Filtering (first iteration on bottom) coherence volumes (1,536 ms). Poststack SOF filter used is a 20 percentile Alpha-Trimmed Mean. Results of the first iteration show a slight improvement in channel edges seen with the blue arrows, but most notably, greatly increased internal channel detail seen with the blue oval. Similarity filter controls are non-aggressive. Overall increase in continuity of previously interpreted channels allows for continued iteration.

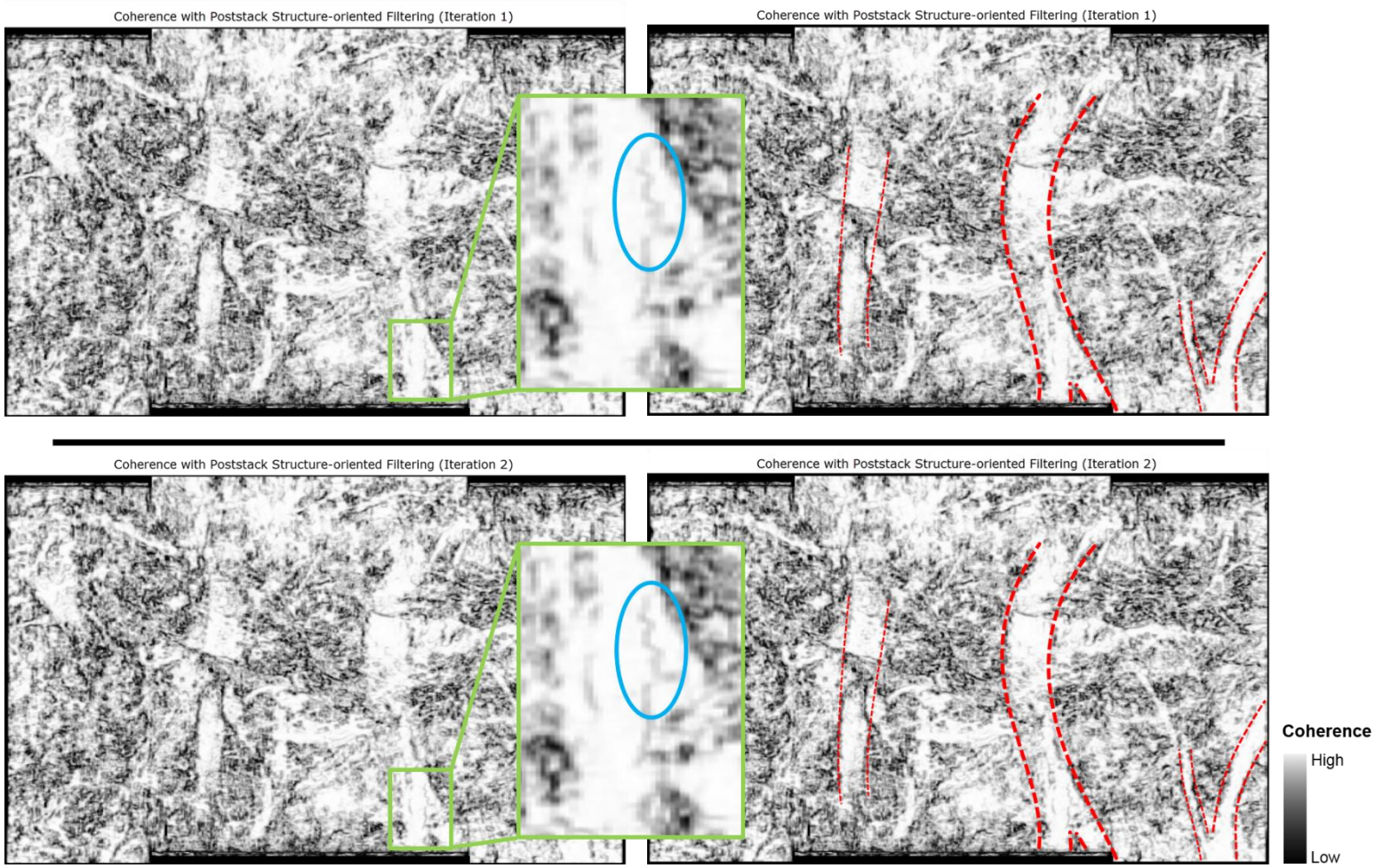

Figure 15. Poststack Structure-oriented Filtering (first iteration on top and second iteration on the bottom) coherence volumes (1,536 ms). Poststack SOF filter used is a 20 percentile Alpha-Trimmed Mean. Results of the second iteration continue to build on the improvements of the first iteration seen in Figure 14, mostly notably edge detection and internal channel detail seen with the blue oval. This step will serve as a stopping point for Poststack Structure-oriented Filtering due to continued iterations resulting in miniscule improvements in channel edge detection.

CHAPTER VI: STRUCTURE ORIENTED FILTERING RESULTS

Prestack Structure-oriented Filtering (SOF) iterations 1 and 2 show improvements in the signal-to-noise ratio, resulting in slight improvements in channel coherence (achieved by the non-aggressive similarity filter controls parameterization), cleaner channel edges, this comes at a minor expense of internal channel detail and finer edge loss. Overall there is an increase in continuity of previously interpreted channels.

Figure 16 display the effect of prestack SOF on seismic amplitude gathers. As a result of the filtering, reflectors are stronger and laterally continuous and noise is removed, however cross-cutting reflectors are still present. Prestack SOF iteration 2 improvements are not noticeable in gather display, those subtle enhancement are best seen in Figure 15.

Poststack SOF iterations 1 and 2 show slight improvement in channel edges, but more notably, greatly increased internal channel detail and its respective edge detection. While poststack SOF offers a smaller pedigree of channel continuity enhancement, it does provides a unique uplift that Prestack SOF does not in terms of subtler internal channel detection.

Final coherence and coherent energy co-rendered results comparing original seismic data and a final processed product can be seen in Figure 17. Seen on the left is the unmuted and unprocessed seismic co-rendered volume, and on right is a volume that has undergone a mute, 2 iteration of Prestack SOF and 2 iterations of Poststack SOF. Blue arrows indicate the increased continuity by lieu of increased coherent energy.

Yellow arrows indicate improved channel edges through a depiction of contrasting continuity/discontinuity seen through coherence. Shown are volumes at 1592 ms that were flattened on the Petrel surface.

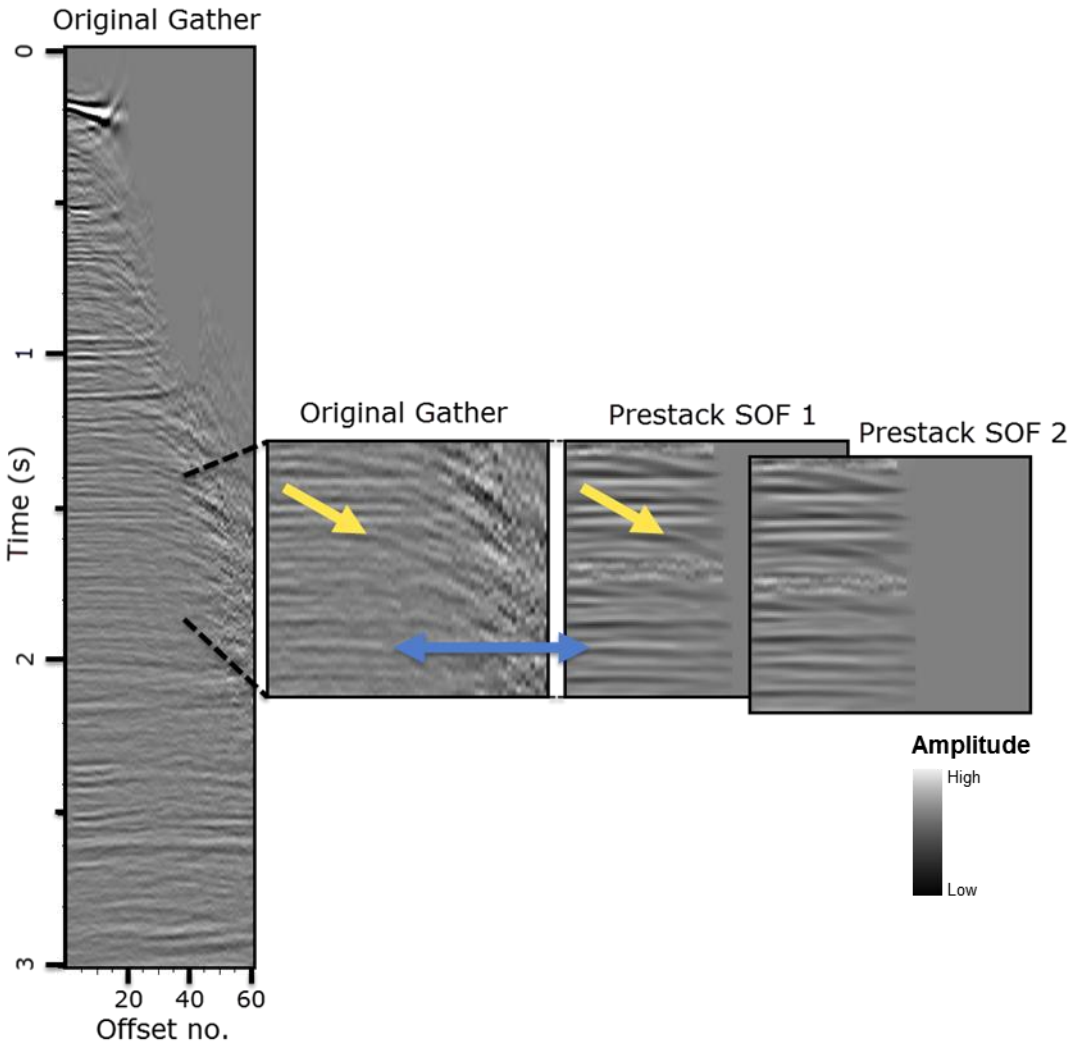

Figure 16. Original and Structure-oriented Filtering iterations 1-2 seismic amplitude gathers panels. From left to right: original gather panel (uncropped and unmuted), cropped original gather panel (time 1,400 to 1,860 ms), Prestack SOF iteration 1, Prestack SOF iteration 2. As a result of the filtering, reflectors are stronger and laterally continuous (shown in blue arrows) and noise is removed, however cross-cutting reflectors are still present (shown in yellow arrows). Prestack SOF iteration 2 improvements are not noticeable in gather display, those subtle enhancement are best seen in Figure 15.

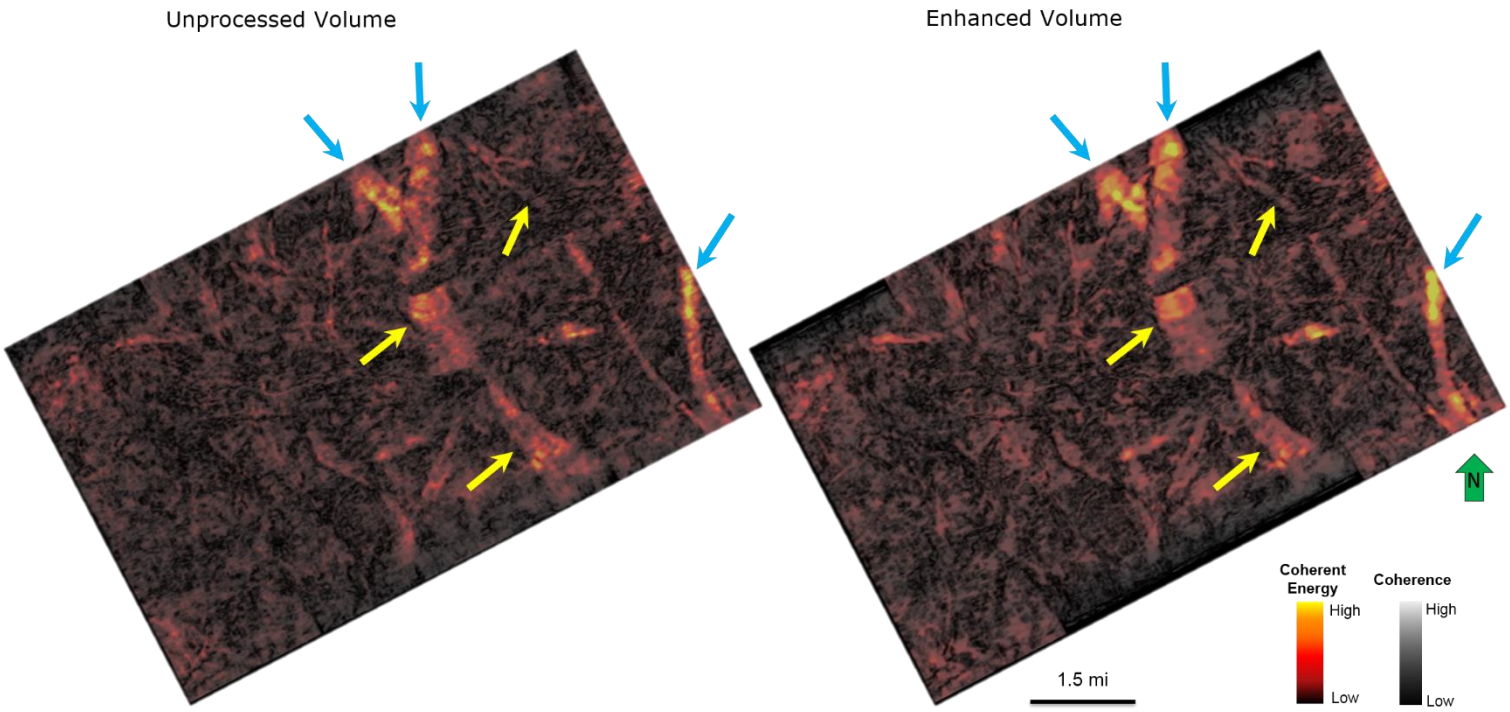

Figure 17. Coherence and coherent energy co-rendered results comparing original seismic data and a final processed product. Seen on the left is the unmuted and unprocessed seismic co-rendered volume, and on right is a volume that has undergone a mute, 2 iteration of Prestack SOF and 2 iterations of Poststack SOF. Blue arrows indicate the increased continuity by lieu of increased coherent energy. Yellow arrows indicate improved channel edges through a depiction of contrasting continuity/discontinuity seen through coherence. Shown are volumes at 1592 ms that were flattened on the Petrel surface.

CHAPTER VII: INTERPRETATIONS

We start by looking at the deepest section of our formation. Figure 18a shows that there is a relatively thin channel present here (1764 ms).A coherence and coherent energy attributes (as a co-render) are used to find these channels as they help delineate discontinuous features. The major channels are highlighted with a blue boundary for better visualization, seen on the right side of Figure 18. As we move up the formation, the channels start getting thicker and wider (1624 ms), which we are able to accurately image with sections of high coherent energy (Figure 18b). The high coherent energy indicates low impedance sands, which could possibly signal the presence of hydrocarbons in these channels. As we approach shallower depths of the Cree Sands (1592 ms), we can see distributary channels with multiple crevasse splays (Figure 18c). Again, we are able to distinguish this with the help of coherence and coherent energy attribute.

The Cree deltaic lobe is characterized by a slow progradation, which displays a number of deltaic facies and changes in channel types, capped by sea level rise. During Aptian time (Figure 19b), sea level is relatively high, and the deepwater/prodelta Naskapi shale is deposited. By the Early Albian (Figure 19c), sea level has begun to drop and the delta front moves forward, with the study areas seeing mainly distal delta channel distributaries. These channels are thinner, such as those in Figure 18a and 18b. During the Mid-Albian (Figure 19d), as the sea level drops further, the study areas sees relatively proximal part of the delta, and the broad channels dominate; this is similar to Figure 18c

and 18d. Finally, during the Late Albian (Figure 19e), sea level increases, and the shale rich pro delta facies of the Sable shale are deposited.

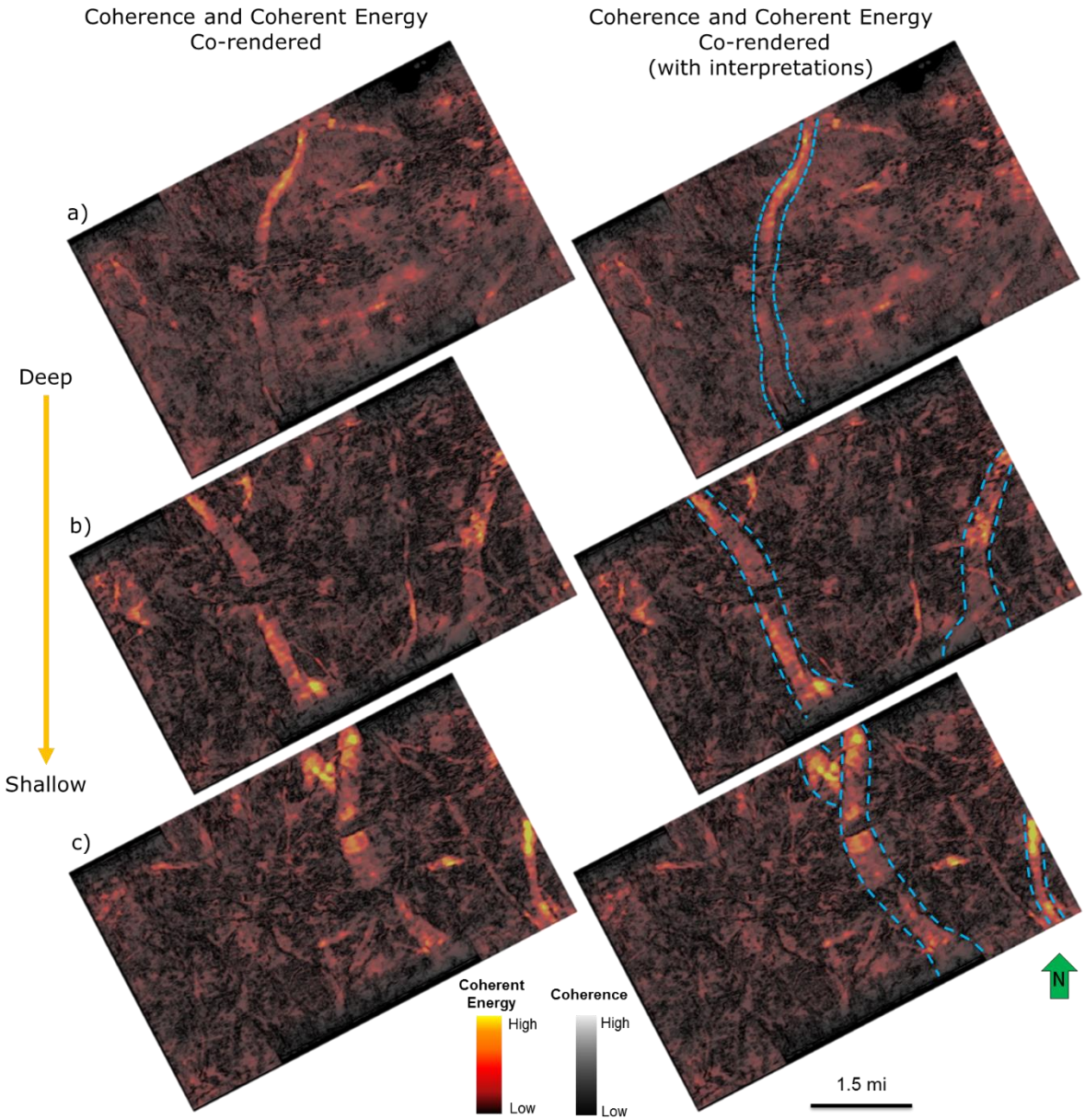

Figure 18. Channel delineation using coherence and coherent energy. All volumes display a co-render of enhanced coherence and coherent energy volumes. On the left are interpreted displays, and the right contains channel interpretations outlined in dashed curved blue lines. Volumes are presented from deep to shallow. On the top (a) there is a relatively thin channel (1764 ms). In the middle (b), as we shallow up we see an increase in channels, as well as, their broadening (1624 ms). In the bottom (c), there is continued broadening of channels, albeit minor (1592 ms). Shown are volumes were flattened on the Petrel surface.

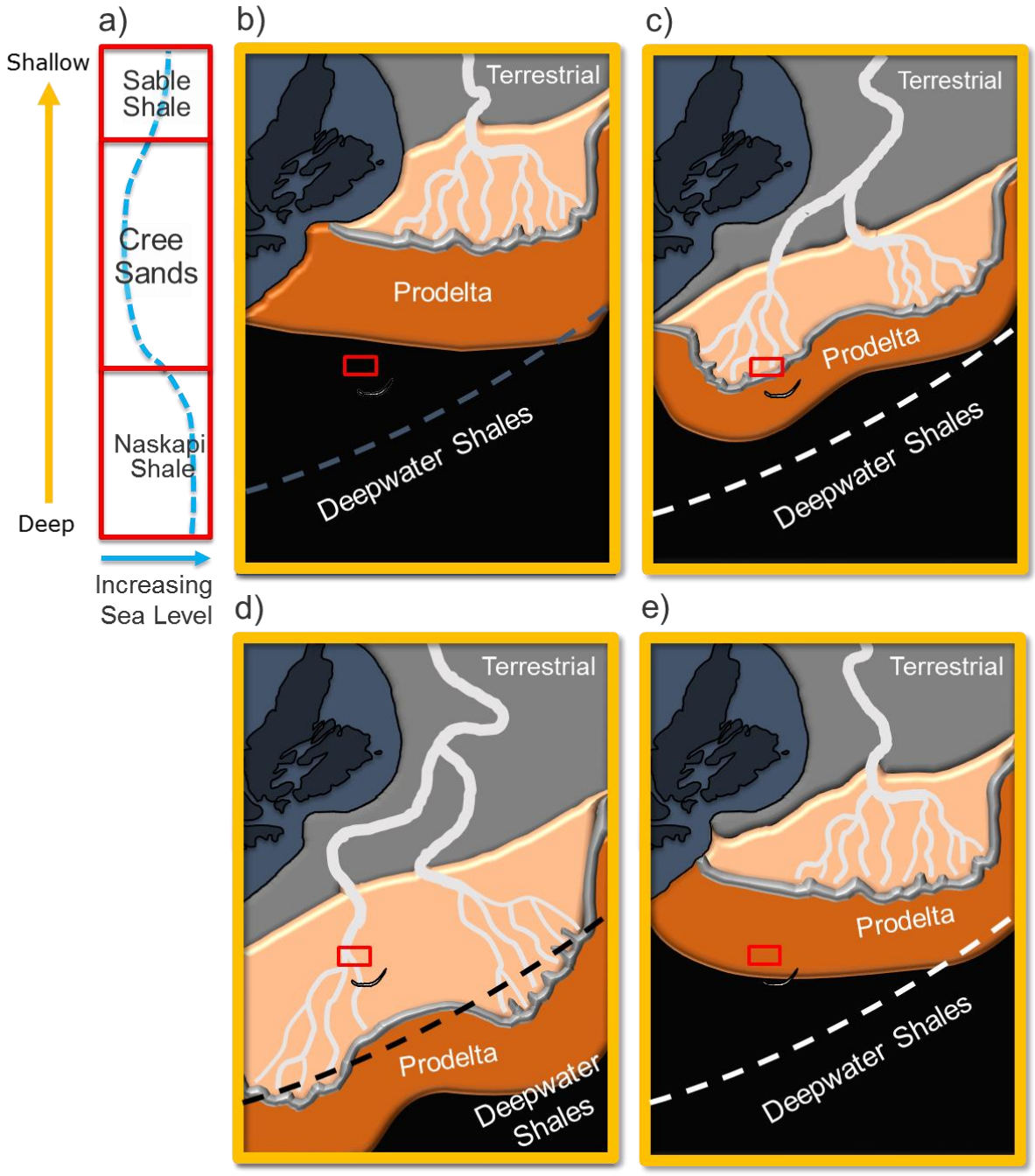

Figure 19. Interpretation of the deltaic channels based on the seismic attribute interpretation. (a) sea level curve, obtained from Haq et al, 1987. (b-d) the changing position of the delta due to sea level, from older to younger. Here, this model is bounded by the red rectangle shown in the Figure 1. The dashed line represents the Aptian paleo shelf break (modified from Khoudaiberdiev et al, 2017).

CHAPTER VIII: CONCLUSIONS

Integrating an analysis of well data allowed for facies change analysis within the area of interest. A fining upward sequence further revealed information on the dominance of channel assemblages at depth.

Muting is an essential first step in the data conditioning workflow. Application of a seismic mute was instrumental in having a positive impact on the signal-to-noise ratio when attempting to gain the best possible image for further processing. By removing traces that are heavily contaminated with noise from a dataset, channel edges become more readily apparent. Further data conditioning from Prestack and Poststack Structure-oriented Filtering (SOF) increase the ability to accurately map channel edges, their respective continuity and also reveal internal channel structures not previously discernable. These improvements are achieved through noise reduction and edge preservation (Zhang et al. 2016).

Similarity seismic attributes (coherence and coherent energy) were used to delineate features of interest, namely deltaic channels. Coherence is an excellent channel edge delineator, and when combined with coherent energy, high coherent energy further distinguishes channels. Utilizing the results from similarity, I was able to use my seismic interpretation to identify different channel assemblages. Based on how these assemblages changed through time, I was able to create the composite interpretation seen in Figure 19. Thus, I was able to use seismic imaging to identify and interpret deposition environment changes within a known deltaic system.

REFERENCES

Bacon, M., Redshaw, T., & Simm, R. (2007). Glossary. In 3-D seismic interpretation (p. 204). Cambridge: Cambridge University Press.

Bhatnagar, P., C. Bennett, R. Khoudaiberdiev, S. Lepard, S. Verma, 2017, Seismic Attribute Illumination of a Synthetic Transfer Zone. SEG Technical Program Expanded Abstracts 2017, 2112–16, 2017. doi.org/10.1190/segam2017-17664850.1.

[CNSOPB] Canada-Nova Scotia Offshore Petroleum Board - Regional Geology Overview, 2008.| Call For Bids Archives. callforbids.cnsopb.ns.ca/2008/01/regional_geology.html.

Chopra, S., K. Marfurt, 2007, Seismic attributes for prospect identification and reservoir characterization: SEG Geophysical Developments No. 11. doi.org/10.1190/1.9781560801900

DelMoro, Y., A. Fernandez, S. Verma, K. Marfurt, 2013, 3-D Surface Seismic Attribute and Prestack Impedance Inversion Characterization of the Red Fork Formation, Oklahoma USA : AAPG Search and Discovery, Article no. 90163.

Google Earth Maps, https://www.google.com/earth/, browsed on March 15, 2017.

Haq, B.U., J. Hardenbol, and P.R. Vail, 1987, Chronology of fluctuating sea levels since the Triassic: Science, 235, 1156-1187.

Khoudaiberdiev, R., C. Bennett, P. Bhatnagar, S. Verma, 2071, Seismic Interpretation of Cree Sand Channels on the Scotian Shelf. SEG Technical Program Expanded Abstracts 2017, 2008–12, 2017. doi.org/10.1190/segam2017-17742372.1.

Mandal, A. and Srivastava, E., 2017. Enhanced structural interpretation from 3D seismic data using hybrid attributes: New insights into fault visualization and displacement in Cretaceous formations of the Scotian Basin, offshore Nova Scotia: Marine and Petroleum Geology, 89 464 - 478.

Marcus P. Cahoj, Sumit Verma, Bryce Hutchinson, and Kurt J. Marfurt, 2016, Pitfalls in seismic processing: An application of seismic modeling to investigate acquisition footprint: Interpretation, 4(2), SG1-SG9. https://doi.org/10.1190/INT-2015-0164.1

[NSDE] Nova Scotia Department of Energy, 2011, Play Fairway Alanysis Atlas – Offshore Nova Scotia, Canada: http://energy.novascotia.ca/oil-and-gas/offshore/play-fairway-analysis/analysis, browsed on March 15, 2017.

Peyton, L., R. Bottjer, and G. Partyka, 1998, Interpretation of incised valleys using new 3D seismic techniques: A case history using spectral decomposition and coherency: The Leading Edge, 17, 1294–1298.

Piper, D. J. "Surficial geology and physical properties 6: deep water surficial geology." 1991, doi:10.4095/210698.

Qayyum, F., Catuneanu, O., Bouanga, C.E, 2015, Sequence stratigraphy of a mixed siliciclastic-carbonate setting, Scotian Shelf, Canada, SEG Interpretation Journal, Volume 3, Issue 2, p. SN21-SN37.

Qayyum, F., de Groot, P., and Hemstra, N., 2012. Using 3D Wheeler diagrams in seismic interpretation - the HorizonCube method. First Break, vol. 30, p. 103-109.

Slatt, R.M., 2006, Stratigraphic reservoir characterization for petroleum geologists, geophysicists, and engineers: Elsevier Publ. Co.

Zhang, B., Lin, T., Guo, S., Davogustto, O. E., & Marfurt, K. J. (2016). Noise suppression of time-migrated gathers using prestack structure-oriented filtering. Interpretation, 4(2), SG19-SG29. doi:10.1190/int-2015-0146.1